

Contents

1	Introduction	1
2	Big-Bang Nucleosynthesis	7
3	Hubble Tension	10
3.1	Standard Λ CDM Model	11
3.2	Λ CDM Model with $\delta v_{\text{rec}} \neq 0$	11
3.3	Remarks	17
4	Axi-Higgs Model	18
4.1	Single-Axion Model	20
4.2	Two-Axion Model	24
5	S_8/σ_8 Tension	25
6	Hubble Tension versus S_8/σ_8 Tension	30
7	Isotropic Cosmic Birefringence	32
8	Testing the Axi-Higgs Model	33
9	Conclusions	37
A	Some Analytical Formulae	38

1 Introduction

Cosmology has made tremendous progress since the mid-20th century, moving from a speculative to a precision science. The inflationary universe scenario, big bang nucleosynthesis (BBN), cosmic microwave background (CMB) and structure formation have merged theory and observational data into a generally accepted picture of our universe.

Two prominent successes in precision cosmology are the measurement of BBN and the determination of Hubble parameter H_0 . However, as more and better data becomes available while theoretical understanding is progressing, tensions (or frictions/conflicts) emerge. They include in particular the four cases listed below.

1. While theoretical estimates for the primordial abundances of helium ^4He and deuterium D in BBN are consistent with the observational data, the theoretical prediction for the primordial Lithium abundance, $^7\text{Li}/\text{H} = (5.62 \pm 0.25) \times 10^{-10}$, is too big compared to its

observed value ${}^7\text{Li}/\text{H}^{\text{obs}} = (1.6 \pm 0.3) \times 10^{-10}$. This $\sim 9\sigma$ discrepancy is known as the ${}^7\text{Li}$ puzzle [1].

2. The determination of the Hubble parameter value from the CMB measurement in Planck 2018 (P18) within the Λ cold dark matter (ΛCDM) model (early universe), namely $H_{0,\text{P18}} = 67.36 \pm 0.54$ km/s/Mpc [2], is smaller than $H_{0,\text{late}} = 73.3 \pm 0.8$ km/s/Mpc, the Hubble parameter value obtained from late-time (with redshift $z < 2$) measurements [3]. This $\sim 4 - 6\sigma$ discrepancy is referred to as the Hubble tension.
3. Recently, a measurement of isotropic cosmic birefringence (ICB) was reported, based on the cross-power (parity-violating) C_l^{EB} data in CMB [4]. It excludes the null hypothesis at 99.2% confidence level (C.L.). This needs to be explained too.
4. The weak lensing measurement of S_8 together with the clustering parameter σ_8 [5] yields a value smaller than that given by the CMB- ΛCDM value. This $\sim 2 - 3\sigma$ [6, 7] discrepancy poses another problem to our understanding of the universe.

In this paper, we present a simple model, with an axion coupled to the Higgs field and hence named ‘‘axi-Higgs’’, to solve or alleviate these four tensions. Let us consider the possibility that the Higgs vacuum expectation value (VEV) in the standard model (SM) of particle physics, $v_0 = 246$ GeV today, is $\sim 1\%$ higher in early universe, *i.e.*, $\delta v_{\text{ini}} = (v_{\text{ini}} - v_0)/v_0 \sim 1\%$ ¹. If the massive gauge bosons, quarks and charged leptons in the SM all have masses about δv_{ini} higher than their today’s values, the discrepancies in the first two cases will be substantially reduced. We propose that a $\delta v > 0$ is the leading effect in modifying the ΛCDM model in the early universe.

That a $\delta v_{\text{BBN}} \gtrsim 1\%$ at BBN time solves the ${}^7\text{Li}$ problem is known [1, 8–17]. That an electron mass $m_e \propto v$ about 1% higher at recombination time (*i.e.*, $\delta m_e \simeq \delta v_{\text{rec}}$) has been suggested to alleviate the Hubble tension [18, 19]. To implement both, the Higgs VEV with $\delta v \sim 1\%$ needs to stay throughout the BBN-recombination epoch (from seconds/minutes to 380,000 years after the Big-Bang) and then drops to its today’s value where its drift rate is $\lesssim 10^{-16}\text{yr}^{-1}$, to satisfy the observational bounds [20–22].

Such a setup can be naturally achieved in string theory. Consider the scenario of brane world in Type IIB string theory, where anti-D3-branes span our three spacial dimensional universe. The SM particles are open-string modes inside the branes. It is known that the electroweak-scale interactions will shift the cosmological constant Λ by many orders of magnitude above its exponentially-small observed value, so fine-tuning is needed to have the right value. In the supergravity (SUGRA) model proposed recently [23], a superpotential $W = X(m_s^2 F(A) - \kappa H_u H_d) + \dots$ is introduced. Here A stands for complex structure (shape) moduli and dilaton

¹In this paper, we will take a set of shorthand notations, including $\Delta X = X - X_{\text{ref}}$, $\delta X = \Delta \ln X$ and $Y_{|X} = \frac{\partial \ln Y}{\partial \ln X}$, $Y_{||X} = \frac{d \ln Y}{d \ln X}$, unless otherwise specified. If $X = \omega_b$, the notations of $Y_{|X}$ and $Y_{||X}$ will be further simplified as $Y_{|b}$ and $Y_{||b}$ etc.

that describe the compactification of extra dimensions and X is a nilpotent superfield which projects the two electroweak Higgs doublets H_u, H_d to the single Higgs doublet ϕ . This leads to the axi-Higgs model,

$$V = m_a^2 f_a^2 \left(1 - \cos \frac{a}{f_a}\right) + |m_s^2 F(a) - \kappa \phi^\dagger \phi|^2, \quad \text{with } F(a) = 1 + C \frac{a^2}{M_{\text{Pl}}^2}. \quad (1.1)$$

In this model, the axion-like field a is a pseudo-scalar component in A . This axion starts with an initial value a_{ini} in early universe. We normalize $F(a)$ to be $F(a=0) = 1$, such that the Higgs VEV $v_0 = \sqrt{2}m_s/\sqrt{\kappa} = 246$ GeV and the Higgs boson mass $m_\phi = 2m_s\sqrt{\kappa} = 125$ GeV. So this model is characterized by four parameters, namely m_a, f_a, C and a_{ini} . The perfect square form of the Higgs potential, where the Higgs contribution to Λ is completely screened by the supersymmetry (SUSY) breaking anti-D3-brane tension m_s^4 , allows a naturally small Λ [24, 25]. Notably, this perfect square form of the Higgs potential, together with the damping effect of the Higgs decay width ($\Gamma_\phi \simeq 4$ MeV), is crucial in yielding the desirable feature of the model: the effect of the Higgs field evolution is totally negligible in the axion evolution, but the axion evolution significantly affects the evolution of the Higgs VEV.

Starting with an initial $\delta v_{\text{ini}} = C a_{\text{ini}}^2 / 2M_{\text{Pl}}^2$ via the mis-alignment mechanism for $a_{\text{ini}} \neq 0$, δv evolves after the recombination epoch ($z \sim 10^3$) when $3H(t)$ drops below m_a . We find the favored axion mass

$$m_a \sim 10^{-30} - 10^{-29} \text{ eV}. \quad (1.2)$$

Here the upper limit of m_a is determined by whether δv will drop too much by the time of recombination, which happens for $m_a > 3.3 \times 10^{-29}$ eV. The lower limit of m_a , instead, is set by the late-time measurements of $\delta v(t)$ or its drift rate. The current atomic clock (AC) measurements on $d(\delta v)/dt|_{t_0}$ [22] excludes $m_a \lesssim 1.6 \times 10^{-30}$ eV at 95% C.L. Such a mass scale is compatible with string theory and typical axion masses [26, 27]. Note that it is very difficult to satisfy the AC bound today if we introduce a scalar field φ instead, as $F(\varphi)$, a counterpart of $F(a)$ in Eq. 1.1, will contain a linear term with a coefficient too big in the absence of fine-tuning.

Physically, an upward variance of the Higgs VEV will reduce Y_p but raise D/H. The current experimental bounds on Y_p and D/H are still compatible with a change of percent level in v if η is also 1 – 2% larger than its reference value 6.127×10^{-10} [2, 28]. Beyond that, it is suggested in [8, 10, 13, 17] that the ${}^7\text{Li}$ problem can be greatly alleviated if the light quarks are $\sim 1\%$ heavier during the BBN epoch. Following this, we find that addressing the ${}^7\text{Li}$ problem yields

$$\delta v_{\text{BBN}} = (1.1 \pm 0.1)\%, \quad \delta \eta = (1.7 \pm 1.3)\%. \quad (1.3)$$

Here the baryon density ω_b is about 1.7% higher than the value obtained from the P18 data.

We then introduce an analytical formalism to study the impacts of $\delta v_{\text{rec}} = \delta v_{\text{BBN}} \sim 1.1\%$ for the combined P18+BAO (Baryon Acoustic Oscillation) predictions [29] using the original fitting results of ΛCDM as a reference [2]. Since δv_{rec} is small, we treat its effects perturbatively.

We demand the angular sound horizon θ_* at the recombination to be preserved while the $r_d h$ value to be shifted from its CMB value to its BAO value, when δv_{rec} is turned on. Here r_d is the sound horizon at baryon decoupling epoch and h is the dimensionless Hubble parameter. Then with the inputs from the linear BBN analysis, namely $\delta v_{\text{rec}} = \delta v_{\text{BBN}}$ and $\delta\omega_b = \delta\eta$, we eventually find

$$H_0 = H_{0,\text{P18}}(1 + h_{\parallel v} \delta v_{\text{rec}}) = 69.03 \pm 0.61 \text{ km/s/Mpc} . \quad (1.4)$$

Here H_0 is derived from its reference value $H_{0,\text{P18}}$ (see Sec. 3) and its error mostly comes from the BAO uncertainty. This H_0 value alleviates the tension with its late-time measurements. It is consistent with the numerical analysis taken by Planck 2015 [18] and Hart & Chluba [19]. However, as we shall see, this may not be the whole story on H_0 in the axi-Higgs model.

The existence of this axion introduces an axion matter density $\omega_a > 0$ and hence contributes to the CDM today. Because of its very big de Broglie wavelength ($\sim 10^3$ Mpc), this axion tends to suppress the matter power spectrum. The S_8/σ_8 prediction by the CMB data is then shifted down from its previously determined value. The weak-lensing and the CMB measurements are thus reconciled to some extent, with

$$x \equiv \frac{\omega_a}{\omega_m} \sim 1\% \quad (1.5)$$

or

$$a_{\text{ini}} \sim 10^{17} - 10^{18} \text{ GeV} . \quad (1.6)$$

Being an ultra-light axion, the coupling of a to two photons naturally introduces an ICB effect in the CMB, at a level in agreement with the recently observed C_l^{EB} spectrum [4]. In the data fitting, we determine (as in $aF_{\mu\nu}\tilde{F}^{\mu\nu}/32\pi^2 f_a$)²

$$\frac{a_{\text{ini}}}{f_a} \simeq 1.0 \pm 0.3 \quad (1.7)$$

and hence

$$f_a \simeq 10^{17} - 10^{18} \text{ GeV} , \quad (1.8)$$

with an input of Eq. (1.6). Since $a_{\text{ini}}/f_a < \pi$, the axion rolls towards $a = 0$ instead of $a = 2\pi$. This explanation as one possibility is already known [30–32], though our determination of the parameters comes from an entirely different direction and is much more precise in terms of the axion properties. Here, one may be tempted to identify $f_a \simeq M_{\text{Pl}} = 2.4 \times 10^{18}$ GeV.

In summary, the axion density ω_a determines the value of a_{ini} , while the initial variation of the Higgs VEV δv_{ini} determines the value of $C a_{\text{ini}}^2$. The axion mass m_a is determined by the

²Fitting the ICB data requests the a_{ini} values to be negative. Here we simply drop this minus sign for the convenience of presentation, since the cosmological problems to be addressed in this paper, except this one, are not sensitive to this sign (protected by a Z_2 symmetry of $a \rightarrow -a$ for the axion Lagrangian in Eq. (1.1)).

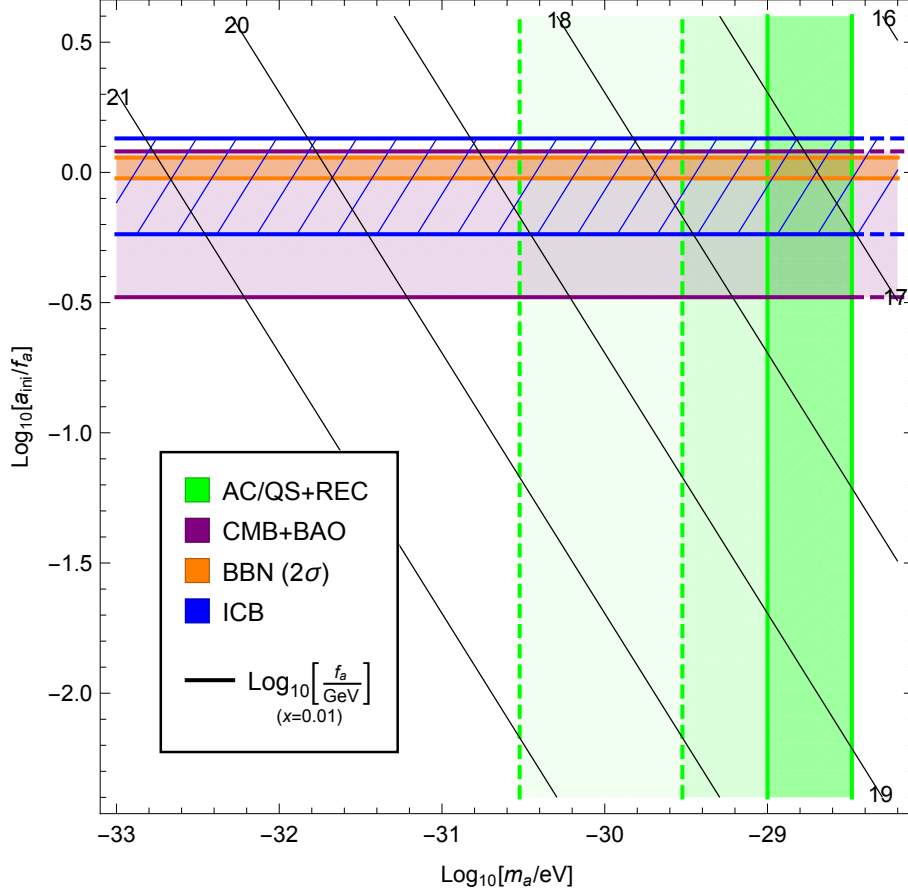


Figure 1: Overall picture on the axi-Higgs cosmology with single axion. The axion mass is bounded from above by requiring the axion not to roll down until near or after the recombination, and limited from below by the AC measurements on m_e/m_p drift rate [22] (solid-green). The projected lower limits from astronomical observations of molecular absorption spectra, in terms of the present and the two-order improved precisions for eighteen known quasars [33], are also presented (dashed-green). The CMB+BAO data, previously encoded in the Λ CDM+ m_e context to address the Hubble tension [19], is recast in this axi-Higgs model (with $C' = 0.01$). The BBN data fitting is shown at 2σ C.L. (1σ C.L. is taken for the others) for better demonstration. In the favored parameter region, the ${}^7\text{Li}$ puzzle is largely solved. The recently reported ICB anomaly [4] also gets explained in this model. We draw the contours of f_a with $x = 0.01$, a value suggested to mitigate the S_8/σ_8 tension. In the intersection region of all, f_a is favored to be $\sim 10^{17} - 10^{18}$ GeV.

requirements that δv_{ini} stays unchanged (or mildly changed) until near or after the recombination and oscillates with a highly-suppressed amplitude at low redshift and today, while f_a is determined by the ICB data. The four parameters parametrizing this axi-Higgs model are determined up to an order of magnitude at 1σ C.L. Note that the impact of δv_{ini} in BBN is mostly in quark (and nucleon) and W -boson masses, while its impact on the CMB is mostly via electron mass m_e . Fortunately, they are intimately linked in the SM of particle physics, where the particle masses are proportional to v . Overall, the properties of the axi-Higgs model in addressing the four issues are presented in Fig. 1. For the convenience of presentation, we take a redefinition of $F(a) = 1 + C'a^2/f_a^2$, with $C' = Cf_a^2/M_{\text{Pl}}^2$.

Note that the evolution of δv is described by the physics of a damped oscillator. The oscillating feature of δv may be detected by the AC measurements [20–22], while its non-zero value may be detected by the quasar (QS) spectral measurements [33]. With further improvements in their precisions in the near future, the axi-Higgs model should be seriously tested.

Notably, though the Hubble tension and the S_8/σ_8 tension can be alleviated in the single-axion case, by turning on δv_{rec} and x respectively, some trade-off effect exists between relaxing the Hubble and S_8/σ_8 tensions. Turning on δv_{rec} alone exacerbates the S_8/σ_8 tension while turning on x alone exacerbates the Hubble tension. This effect could be suppressed by introducing a second axion. Recall in the the fuzzy dark matter (FDM) scenario [26, 34–36], where the problems such as cusp-core, too many satellites etc. confronting the weakly-interacting-massive-particle scenario, an axion a_2 with its mass $m_2 \sim 10^{-22}$ eV comprises the CDM. In the axi-Higgs model with two axions, $F(a)$ extends to

$$F(a_1, a_2) = 1 + C_1 \frac{a_1^2}{M_{\text{Pl}}^2} + C_2 \frac{a_2^2}{M_{\text{Pl}}^2}, \quad (1.9)$$

where a_1 should be recognized as the counterpart of the a field (see Eq. (1.2)). The FDM axion a_2 starts with $a_{2,\text{ini}}$ at the BBN time and rolls down at a redshift z_2 with $z_{\text{rec}} \ll z_2 \simeq 2.0 \times 10^6 \ll z_{\text{BBN}}$. The present CDM density ω_c determines the value of $a_{2,\text{ini}}$. So the a_2 contribution in $F(a_1, a_2)$ is important at the BBN epoch but becomes negligible at the recombination time. In this context, $\delta v_{\text{rec}} > \delta v_{\text{BBN}}$ is allowed with a negative C_2 . With this additional parameter (C_2 or δv_{rec}), we find that a choice of

$$\delta v_{\text{rec}} \sim 4\% \quad \text{and} \quad x \sim 2\% \quad (1.10)$$

may better resolve the Hubble and S_8/σ_8 tensions, with δv_{BBN} remaining 1.1%. An analysis beyond our linearized approach and with a full treatment of the CMB+BAO data will be important to pin down more precise values.

The rest of the paper goes as follows: Sec. 2 covers the BBN epoch. Choosing $\delta v_{\text{ini}} = 1.1\%$ reduces the theoretical prediction for ${}^7\text{Li}/\text{H}$, mostly due to the caused modifications to the strong/nuclear interaction rates. Sec. 3 discusses the H_0 value with the input of $\delta v_{\text{rec}} = \delta v_{\text{BBN}}$.

We present an analytical discussion, referring to [19] for a numerical analysis. Feeding in the BBN values for δv and ω_b , we determine the upshift of H_0 from its P18 value. Sec. 4 presents a simple axi-Higgs model suggested by string theory on how the Higgs VEV evolves from $v_{\text{ini}} = v_0(1 + \delta v_{\text{ini}})$ to v_0 today, predicting the existence of an axion with mass $m_a \sim 10^{-30} - 10^{-29}$ eV. Sec. 5 discusses the impact of the axion density ω_a on the CMB measurements of S_8/σ_8 . Sec. 6 discusses the trade-off effect between relaxing the Hubble and S_8/σ_8 tensions, where the two-axion model comes in handy. Sec. 7 discusses how this axion explains the recently reported ICB anomaly, with $f_a \simeq a_{\text{ini}} \sim 10^{17} - 10^{18}$ GeV. Section 8 discusses the testing of the axi-Higgs model in the near future, via the AC and/or QS measurements. Sec. 9 contains the conclusion and some remarks. The appendix provides some technical details on the CMB/BAO analyses in the main text.

2 Big-Bang Nucleosynthesis

BBN occurs during the radiation-dominant epoch, with a typical temperature scale of $\mathcal{O}(1-0.1)$ MeV, when the radiation becomes too soft to significantly break the generated light chemical elements or bound states of nucleons. Locally, the primordial abundances of these elements can be extrapolated from optical observations, such as the absorption lines of ionized hydron region in compact blue galaxies [37], the QS light passing through distant clouds [38], and the spectra of metal-poor main-sequence stars [39]. Most of the measured values match with their theoretical prediction based on standard Λ CDM model with very high precision, except a discrepancy about 9σ appearing for ${}^7\text{Li}$. This is often named the ${}^7\text{Li}$ puzzle [40]. We present the primordial abundances of ${}^4\text{He}$, D and ${}^7\text{Li}$, including their theoretical predictions and astrophysical measurements, in Tab. 1. Notably, the consistency between the observed ${}^4\text{He}$ and D primordial abundances and their theoretical predictions strongly constrains the model space to address this puzzle (for some recent efforts, see e.g. [8, 17, 41–45]). Below we will discuss the impacts of a percent-level shift in Higgs VEV for BBN.

The shift of Higgs VEV from its current value ~ 246 GeV impacts BBN mainly by modifying the following parameters in particle physics.

- Fermi constant $G_F \propto v^{-2}$, or equivalently $m_W \propto v$. The change to m_W modifies all weak interactions, such as the $n \rightleftharpoons p$ conversion and the neutron lifetime. A larger m_W leads to an earlier freeze out of the $n \rightleftharpoons p$ conversion and a longer neutron lifetime. It introduces a larger neutron density than that in the standard BBN picture and thus higher light-element abundances.
- Electron mass $m_e \propto v$. m_e also plays an important role in weak interactions. A larger m_e will reduce the rate of the $n \rightleftharpoons p$ conversion and delay neutron decay. Additionally, it may

	Prediction [28]	Observation [46]
Y_p	0.2471 ± 0.0002	0.245 ± 0.003
$D/H \times 10^5$	2.459 ± 0.036	2.547 ± 0.025
${}^7\text{Li}/H \times 10^{10}$	5.62 ± 0.25	1.6 ± 0.3

Table 1: Primordial abundances of ${}^4\text{He}$, D and ${}^7\text{Li}$: theoretical predications and astrophysical measurements. Here we take the convention in [46]. In particular, $Y_p \equiv \rho({}^4\text{He})/\rho_b$ is the primordial mass fraction of ${}^4\text{He}$ and $D({}^7\text{Li})/H$ represents that the D(${}^7\text{Li}$) primordial abundances relative to that of H. The theoretical predictions are based on the CMB baryon-to-photon ratio $\eta = 6.091 \times 10^{-10}$ [28, 47].

Y \ X	m_W [10]	m_e [10]	Δm_q [10]	\bar{m}_q [13, 17]	η
Y_p	2.9	0.40	-5.9	-1.0	0.039
D/H	1.6	0.59	-5.3	10	-1.6
${}^7\text{Li}/H$	1.7	-0.04	-5.3	-60	2.1

Table 2: Numerical values of $Y_{|X} \equiv \frac{\partial \ln Y}{\partial \ln X}$ for Y_p , D/H and ${}^7\text{Li}/H$. The $Y_{|\Delta m_q}$ values are calculated like [10], but using the lattice average in [48] instead. This modification introduces a rescaling factor ~ 1.16 to the numbers in [10]. The $Y_{|\bar{m}_q}$ values are taken from [13, 17], which are derived based on the $E_B - \bar{m}_q$ relation presented in [49]. Here E_B is nucleus binding energy.

reheat more the photon bath before BBN via electron-positron annihilation.

- Mass difference between up and down quarks $\Delta m_q \equiv m_d - m_u \propto v$. The isospin-breaking Δm_q effect contributes to the mass splitting between neutron and proton Δm_{np} [48], while the latter impacts the $n \rightleftharpoons p$ conversion and neutron decays oppositely, relative to m_W and m_e , as the Higgs VEV varies.
- Averaged light quark mass $\bar{m}_q \equiv (m_u + m_d)/2 \propto v$. The change of \bar{m}_q may significantly influence the rates of strong/nuclear interactions. Heuristically, the effect of increasing \bar{m}_q is manifested an enlarged pion mass m_π . From chiral perturbation theory, we have the well-known relation $m_\pi^2 \simeq \bar{m}_q \langle q\bar{q} \rangle / f_\pi^2$, where f_π is the pion decay constant and $\langle q\bar{q} \rangle$ is the VEV of quark condensate. Since pions are the main mediators between nucleons, a larger m_π makes nuclei less tightly bound. The nuclear-reaction rates thus may change substantially. Here we follow the discussions in [13, 17, 49, 50]. Note, nucleon mass also changes with \bar{m}_q . But this effect is subleading in this context, since the nucleon mass receives contributions mostly from QCD interaction.

Aside from these tree-level impacts, the variation of Higgs VEV can also shift coupling constants, such as α or α_s , or some other physical quantities like neutrino mass. But, these effects are either of next-to-leading order or highly model-dependent. So we will not consider them in this study.

We summarize the $Y_{|X}$ values for Y_p , D/H and ${}^7\text{Li}/\text{H}$ in Tab. 2. These values measure the dependence of the ${}^4\text{He}$, D and ${}^7\text{Li}$ primordial abundances on the Higgs-VEV-mediated parameters discussed above and the baryon-to-photon ratio. As expected, the $Y_{|\Delta m_q}$ values are universally negative for ${}^4\text{He}$, D and ${}^7\text{Li}$. This distinguishes them from most of the $Y_{|m_W}$ and $Y_{|m_e}$ values by a sign. The only exception is $({}^7\text{Li}/\text{H})_{|m_e}$. Due to the extra impact of the variation of m_e on the photon bath and hence the generation of ${}^7\text{Li}$ through the photon-associated ${}^7\text{Be}$ production [28], its value turns out to be slightly negative. Another observation is that the $({}^7\text{Li}/\text{H})_{|\bar{m}_q}$ value is highly negative. This effect can significantly reduce the predicted ${}^7\text{Li}$ primordial abundance given a positive δv_{BBN} or an enlarged \bar{m}_q , and hence lays out the footstone of addressing the ${}^7\text{Li}$ puzzle in this context. We also present the values of $Y_{|\eta}$ in this table. η determines baryon number density during the BBN epoch, and influence BBN directly. As an outcome, we find

$$Y_p(\delta v_{\text{BBN}}, \delta\eta) \simeq Y_p(0, 0)(1 - 3.6\delta v_{\text{BBN}} + 0.039\delta\eta) , \quad (2.1)$$

$$\text{D}/\text{H}(\delta v_{\text{BBN}}, \delta\eta) \simeq \text{D}/\text{H}(0, 0)(1 + 6.9\delta v_{\text{BBN}} - 1.6\delta\eta) , \quad (2.2)$$

$${}^7\text{Li}/\text{H}(\delta v_{\text{BBN}}, \delta\eta) \simeq {}^7\text{Li}/\text{H}(0, 0)(1 - 64\delta v_{\text{BBN}} + 2.1\delta\eta) . \quad (2.3)$$

We present the linear-order constraints on δv and $\delta\eta$ at 1σ C.L. in Fig. 2. In the standard BBN scenario, the ${}^7\text{Li}$ puzzle can be manifested as an η value away from the CMB favored one with ΛCDM . We demonstrate this in this figure as a separation between the orange error bar and the point of $\delta\eta = 0$ along the line with $\delta v_{\text{BBN}} = 0$. The story is dramatically changed in the model with varying Higgs VEV. As δv_{BBN} increases, the $\delta\eta$ value favored by ${}^7\text{Li}/\text{H}$ gets close to zero quickly. The black circle, we will show later which fits the CMB data well and hence can be interpreted as new theoretical prediction approximately, is within 1σ range of the observed ${}^7\text{Li}/\text{H}$! The best fit of δv and $\delta\eta$ to Y_p , D/H and ${}^7\text{Li}/\text{H}$ now reads:

$$\delta v_{\text{BBN}} = (1.1 \pm 0.1)\% , \quad \delta\eta = (1.7 \pm 1.3)\% . \quad (2.4)$$

The reduced χ^2 value at this best-fit point is ~ 7.0 , yielding a fit at $\sim 2.5\sigma$ level. As a comparison, the data can be fitted in the standard BBN scenario only with a χ^2 value ~ 42 or at $\sim 8.8\sigma$ level. The ${}^7\text{Li}$ puzzle is indeed greatly relieved in this new model. Notably we have not taken into account non-linear effects of $\delta\eta$ and δv_{BBN} in these discussions. While $|\delta\eta|$ being far from zero, its non-linear effects might not be negligible. We thus use dashed lines to represent the boundaries of the shaded regions with $|\delta\eta| > 0.2$ in this figure. This explains why the orange belt, obtained by fitting the observed ${}^7\text{Li}/\text{H}$, fails to pass the orange error bar at $\delta v_{\text{BBN}} = 0$. Also, with non-linear effects for δv_{BBN} being incorporated, a slightly bigger value will be favored for δv_{BBN} [17] and hence for $\delta\eta$, we have

$$\delta v_{\text{BBN}} = (1.2 \pm 0.2)\% , \quad \delta\eta = (2.3 \pm 1.4)\% . \quad (2.5)$$

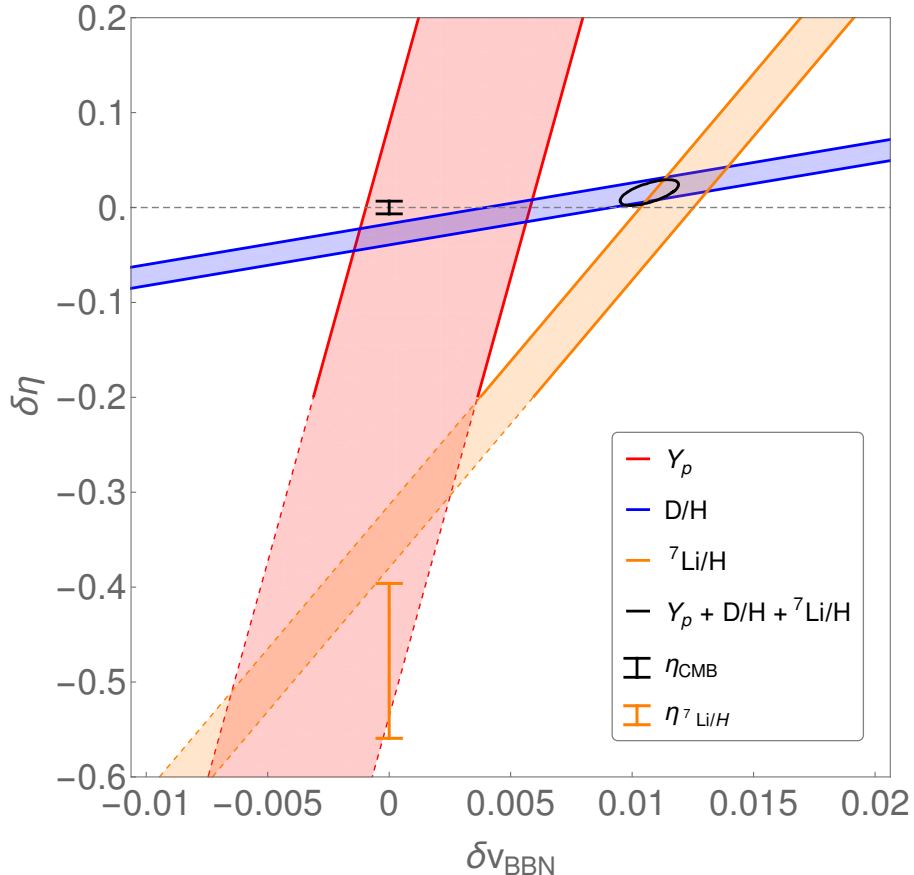


Figure 2: Constraints on δv_{BBN} and $\delta\eta$ at 1σ C.L. Here the black error bar ($\eta_{\text{CMB}} = 6.127 \pm \times 10^{-10}$ at $\delta v_{\text{BBN}} = 0$), namely the interpretation of P18 data in the ΛCDM [2], represents theoretical prediction from standard cosmology.

3 Hubble Tension

Our today’s universe is well-described by Robertson-Walker metric, where its energy density is comprised of about 5% baryons, 25% CDM (be it weakly interacting massive particles or ultra-light axion) and 70% dark energy Λ . However, today’s cosmic expansion rate H_0 from CMB (i.e., the early universe’s prediction) is substantially smaller than the late-time determination, yielding a $\sim 4 - 6\sigma$ discrepancy. We like to examine how a slightly larger Higgs VEV ($\delta v_{\text{rec}} \sim 1\%$) at the recombination epoch impacts on the CMB prediction on H_0 . Since δv_{rec} is small, we shall treat its effects on the Hubble parameter H_0 , the matter density ω_m and the shift in the recombination redshift z_* perturbatively, at a linear level. This allows us to study this problem analytically, so one can get a clearer picture than what a numerical multi-parameter fit provides. Feeding in the baryon density ω_b and δv_{BBN} determined from the BBN analysis and keeping unchanged the observed input data from P18 + BAO, we obtain an upward shift of H_0 relative to the P18+BAO reference value. Our results are consistent with the numerical study by Hart and

Chluba [19]. However, there is some subtlety related to how and what BAO data is applied.

3.1 Standard Λ CDM Model

In the standard Λ CDM model, the dimensionless parameters are defined as

$$\omega_i = \Omega_i h^2, \quad \Omega_i = \frac{\rho_{i,0}}{\rho_{cr,0}}, \quad \rho_{cr,0} = \frac{3H_0^2}{8\pi G}, \quad h = \frac{H_0}{(100 \text{ km/s/Mpc})}, \quad (3.1)$$

for the universe today. We use the subscript γ , ν , b , c , m and r to represent photon, neutrino, baryon, CDM, total matter and radiation, respectively. Then the radiation and total matter energy densities, Λ and Hubble parameter evolve as

$$\rho_r(z) = \rho_{r,0}(1+z)^4, \quad \rho_m(z) = \rho_{m,0}(1+z)^3, \quad \rho_\Lambda = \text{const}, \quad (3.2)$$

$$H(z) = H_0 \sqrt{\Omega_r(1+z)^4 + \Omega_m(1+z)^3 + \Omega_\Lambda}. \quad (3.3)$$

Here the number of relativistic D.O.F. is assumed to be a constant, since we are interested in the late-time universe.

We define the reference model used in this paper as the baseline Λ CDM fitted with P18 data [2]. The cosmological parameters in this reference model then read ³

$$\omega_{b,\text{P18}} = 0.02238, \quad \omega_{c,\text{P18}} = 0.1201, \quad h_{\text{P18}} = 0.6732, \quad Y_{\text{P18}} = 0.2454. \quad (3.4)$$

While ω_b , ω_c and h are subject to vary in the data fitting, we fix the radiation and neutrino sectors with

$$\omega_{\gamma,\text{P18}} = 2.47 \times 10^{-5}, \quad \omega_{\nu r,\text{P18}} = 1.15 \times 10^{-5}, \quad \omega_{\nu m,\text{P18}} = 0.64 \times 10^{-3}. \quad (3.5)$$

These inputs can be inferred from the setup: $T_0 = 2.7255$ K, $N_{\text{eff}} = 3.046$ and $\sum m_\nu = 0.06$ eV. $\omega_{\nu r}$ and $\omega_{\nu m}$ denote massless and massive neutrino densities here. The massive neutrino is modeled as radiation in the early universe and matter at late time [51]. The redshift for its transition is determined by the condition $T_\nu(z_\nu) = \sum m_\nu$, which yields $z_\nu \simeq 356.91$.

3.2 Λ CDM Model with $\delta v_{\text{rec}} \neq 0$

In this subsection we will examine how a variation of Higgs VEV in the recombination epoch impacts the CMB prediction for the value of H_0 and some other cosmological parameters. We will

³Explicitly, we take the best-fit values of ω_b, ω_c and h from Planck 2018 TT,TE,EE+lowE+lensing and derive the values of other physical parameters (*i.e.*, z_* , r_* , D_* , θ_* , z_d , r_d , η) from them. These reference values are denoted with a subscript ‘‘P18’’ later on. Due to our simplified modeling of massive neutrino, slight difference exists in general between the reference value and the central value obtained from marginalization of Planck 2018 data [2], for these parameters.

treat its effects to be perturbative. This allows us to address the Hubble tension analytically and postpone a comprehensive numerical analysis to a later time. We will assume that the variation of Higgs VEV steadily lasts from BBN to at least recombination and hence we have $\delta v_{\text{rec}} \approx \delta v_{\text{BBN}}$. Also, we will choose ω_b , ω_c , h and v as the free parameters for the convenience of discussions below.

As a start, let us consider two CMB/BAO observables. The first one is angular sound horizon, defined as

$$\theta_* = \frac{r_*}{D_*} . \quad (3.6)$$

Here r_* and D_* are the sound horizon and the comoving diameter distance at the recombination (we use “ $*$ ” to denote quantities at the recombination in this paper). They are calculated respectively by

$$r_* = \int_{z_*}^{\infty} dz \frac{c_s(z)}{H(z)} = \mathcal{D} \int_{z_*}^{\infty} dz \left/ \sqrt{3 \left[1 + \frac{3\omega_b}{4\omega_\gamma} (1+z)^{-1} \right] [\omega_r(1+z)^4 + \omega_m(1+z)^3 + \omega_\Lambda]} \right. , \quad (3.7)$$

$$D_* = \int_0^{z_*} dz \frac{1}{H(z)} = \mathcal{D} \int_0^{z_*} dz \left/ \sqrt{\omega_r(1+z)^4 + \omega_m(1+z)^3 + \omega_\Lambda} \right. , \quad (3.8)$$

with $c_s = 1/\sqrt{3(1+3\rho_b/4\rho_\gamma)}$ and $\mathcal{D} = 2998$ Mpc. The angular sound horizon determines the separation of acoustic peaks and troughs of the CMB power spectrum. With the CMB data [2], its value has been measured in the Λ CDM model with a high precision, as

$$(\theta_*)_{\text{CMB}} = (1.04110 \pm 0.00031) \times 10^{-2} . \quad (3.9)$$

Its reference value is calculated as (with $z_{*,\text{P18}} = 1089.87$).

$$(\theta_*)_{\text{P18}} = 1.04100 \times 10^{-2} . \quad (3.10)$$

Another observable is related to the BAO scale which is imprinted on the matter power spectrum. This feature has been measured directly with large-scale structure surveys [29]⁴ and indirectly with the CMB data [2], yielding

$$(r_d h)_{\text{BAO}} = (99.95 \pm 1.20) \text{ Mpc} , \quad (r_d h)_{\text{CMB}} = (99.08 \pm 0.92) \text{ Mpc} , \quad (3.11)$$

where $r_d = \int_{z_d}^{\infty} dz c_s(z)/H(z)$ denotes sound horizon at the end of baryon drag epoch (please find details on the computation of z_* and z_d in Appendix A). The reference value for $r_d h$ is then chosen to be (with $z_{d,\text{P18}} = 1059.95$)

$$(r_d h)_{\text{P18}} = 99.01 \text{ Mpc} . \quad (3.12)$$

⁴This result is inferred from the BAO features of matter power spectrum combining the high-redshift ($z > 0.6$) data [52] including LRGs and ELGs [53,54], QSO [55], Lyman- α forest samples [56] and the low red-shift galaxy data from 6dF [57] and MGS (SDSS DR7) [58].

Y \ X	ω_b	ω_c	h	z_*/d
r_*	-0.1351	-0.2080	-4×10^{-10}	-0.6563
D_*	-0.0624	-0.3349	-0.1934	+0.0151
r_d	-0.1372	-0.2100	-4×10^{-10}	-0.6521

Table 3: Numerical values of $Y_{|X}$ for the cosmological parameters.

The variation of Higgs VEV changes electron mass m_e and hence physics at atomic scale. This will necessarily impact the CMB predictions for cosmological parameters if it happens in the recombination epoch. To extract this out, let us consider how θ_* and $r_d h$ interplay with δv_{rec} . By varying these two observables, we find

$$\begin{aligned} d \ln r_* - d \ln D_* &= d \ln \theta_* , \\ d \ln r_d + d \ln h &= d \ln(r_d h) . \end{aligned} \quad (3.13)$$

Here we take θ_* as an observational input so $d \ln \theta_* = 0$. The variations of r_* , D_* and r_d with respect to v are given by (employing the shorthand notation $r_{*||v} \equiv \frac{d \ln r_*}{d \ln v}$, $r_{*|v} \equiv \frac{\partial \ln r_*}{\partial \ln v}$, $r_{*|c} \equiv \frac{\partial \ln r_*}{\partial \ln \omega_c}$ et. al.)

$$r_{*||v} = r_{*|b} \omega_{b||v} + r_{*|c} \omega_{c||v} + r_{*|h} h_{||v} + r_{*|z_*} z_{*||v} \quad (3.14)$$

$$\simeq -0.135 \omega_{b||v} - 0.208 \omega_{c||v} - 0.656 z_{*||v} , \quad (3.15)$$

$$D_{*||v} = D_{*|b} \omega_{b||v} + D_{*|c} \omega_{c||v} + D_{*|h} h_{||v} + D_{*|z_*} z_{*||v} \quad (3.16)$$

$$\simeq -0.062 \omega_{b||v} - 0.335 \omega_{c||v} - 0.193 h_{||v} + 0.015 z_{*||v} , \quad (3.17)$$

$$r_{d||v} = r_{d|b} \omega_{b||v} + r_{d|c} \omega_{c||v} + r_{d|h} h_{||v} + r_{d|z_d} z_{d||v} \quad (3.18)$$

$$\simeq -0.137 \omega_{b||v} - 0.210 \omega_{c||v} - 0.652 z_{d||v} , \quad (3.19)$$

with (for details, see Appendix A)

$$z_{*||v} = z_{*|v} + z_{*|b} \omega_{b||v} + z_{*|c} \omega_{c||v} + z_{*|h} h_{||v} \simeq 1.018 , \quad (3.20)$$

$$z_{d||v} = z_{d|v} + z_{d|b} \omega_{b||v} + z_{d|c} \omega_{c||v} + z_{d|h} h_{||v} \simeq 0.945 .$$

With the explicit forms of r_* , D_* and r_d , and the determination of $z_{*||v}$ and $z_{*|v}$, the relations in Eq. (3.13) are then reduced to

$$-0.055 \omega_{b||v} + 0.1204 \omega_{c||v} + 0.1934 h_{||v} - 0.6838 = 0 , \quad (3.21)$$

$$-0.1687 \omega_{b||v} - 0.2154 \omega_{c||v} + h_{||v} - 0.6163 = (r_d h)_{||v} . \quad (3.22)$$

The system of Eq. (3.21) and Eq. (3.22) compactly encodes the correlation of the parameter variations, namely $\omega_{b||v}$, $\omega_{c||v}$, $h_{||v}$ and $(r_d h)_{||v}$, introduced by the CMB and BAO observations. Next we demonstrate how a bigger Hubble constant can be achieved in this context. Firstly,

among the four unknowns, $\omega_{b|v}$ can be inferred using the BBN fit in Sec 2, assuming that BBN analysis gives the best determination of ω_b . From Eq. (2.4), one can see that $\delta v_{\text{BBN}} \simeq 1.10\%$ yields a shift to η_{BBN} by 1.68%. This results in

$$\omega_{b|v} = \eta_{\text{BBN}|v} = 1.68/1.10 \simeq 1.55 . \quad (3.23)$$

Note that this positive correlation for $\delta\omega_b$ and δv , motivated by solving the ${}^7\text{Li}$ puzzle, is consistent with our anticipation, arising from addressing the Hubble tension with $\delta m_e > 0$ [19]. Next, if $r_d h$ is treated as an observational input, so $(r_d h)_{|v} = 0$, the remaining two unknowns in Eq. (3.21) and Eq. (3.22) are determined as

$$\omega_{c|v} \simeq 3.70, \quad h_{|v} \simeq 1.67 . \quad (3.24)$$

This means that ω_c and h increase roughly by 3.7% and 1.7% respectively for every percent increase in v . But, as indicated in Eq. (3.11), there exists a discrepancy between the BAO and P18 central values of $r_d h$. So we need to include the uncertainty in $r_d h$ to determine the value of $(r_d h)_{|v}$. However, there are more than one way to incorporate the uncertainty in $r_d h$. To be specific, we adopt

$$(r_d h)_{|v} = \frac{[(r_d h)_{\text{BAO}} - (r_d h)_{\text{P18}}]/(r_d h)_{\text{P18}}}{\delta v} \simeq 0.9 \pm 1.1 , \quad (3.25)$$

by assuming that the discrepancy is caused by the δv_{rec} effect in interpreting the CMB data. Here the 1σ uncertainty for $(r_d h)_{|v}$ arises from that of $(r_d h)_{\text{BAO}}$. Interestingly, at this significance level the value of $(r_d h)_{|v}$ is basically positive. This implies that the reduction of r_d will push up the value of h . This alleviates the Hubble tension! Solving again $\omega_{c|v}$ and $h_{|v}$ but now with Eq. (3.25), one obtains

$$\omega_{c|v} \simeq 2.67 \pm 1.31, \quad h_{|v} \simeq 2.31 \pm 0.82 . \quad (3.26)$$

They translates explicitly to

$$\begin{aligned} \omega_c &= \omega_{c,\text{P18}}(1 + \omega_{c|v}\delta v_{\text{rec}}) = 0.1201 [1 + (2.67 \pm 1.31) 0.011] \simeq 0.1236 \pm 0.017 , \\ h &= h_{\text{P18}}(1 + h_{|v}\delta v_{\text{rec}}) = 0.6732 [1 + (2.31 \pm 0.82) 0.011] \simeq 0.6903 \pm 0.0061 . \end{aligned}$$

The CMB-BAO predictions for more benchmark models (BMs) are presented in Tab. 4 and Fig. 3. The late-time measurement of H_0 is taken from [3], which combines the results of SH0ES [59], H0LiCOW [60], MCP [61], CCHP [62], SBF [63] and MIRAS [64]. The BMs are characterized by particular choices of δv and $\delta\omega_b$ to determine $\delta\omega_c$ and δh from the aforementioned reference point.

In the recombination epoch, the most significant effect of δv_{rec} is on electron mass, where $\delta m_e = \delta v_{\text{rec}}$. Indeed, one can see that a similar trend for the favored r_d and h values is shared

Models	v/v_0	ω_b	ω_c	h	r_d
Ref	1.000	0.02238	0.1201	0.6732	147.07
Λ CDM+ m_e +P18+BAO	1.008 ± 0.007 (0.8 ± 0.7)%	0.02255 ± 0.00017 (0.8 ± 0.8)%	0.1208 ± 0.0019 (0.6 ± 1.6)%	0.6910 ± 0.014 (2.6 ± 2.1)%	146.0 ± 1.3 (-0.7 ± 0.9)%
BM ₁	1.011 1.1%	0.02276 1.7%	0.1236 ± 0.0017 (2.9 ± 1.4)%	0.6904 ± 0.0061 (2.6 ± 0.9)%	144.5 ± 0.4 (-1.8 ± 0.3)%
BM ₂	1.010 1.0%	0.02238 0.0%	0.1229 ± 0.0017 (2.3 ± 1.4)%	0.6872 ± 0.0061 (2.1 ± 0.9)%	145.4 ± 0.5 (-1.1 ± 0.3)%
BM ₃	1.000 0.0%	0.02260 1.0%	0.1189 ± 0.0017 (-1.0 ± 1.4)%	0.6793 ± 0.0061 (0.9 ± 0.9)%	147.1 ± 0.5 (0.1 ± 0.3)%
BM _{BBN}	1.011 ± 0.001 (1.1 ± 0.1)%	0.02276 ± 0.00030 (1.7 ± 1.3)%	0.1236 ± 0.0019 (2.9 ± 1.6)%	0.6904 ± 0.0066 (2.6 ± 1.0)%	144.8 ± 0.7 (-1.6 ± 0.5)%
BM _{BBN(NL)}	1.012 ± 0.002 (1.2 ± 0.2)%	0.02290 ± 0.00031 (2.3 ± 1.4)%	0.1243 ± 0.0019 (3.5 ± 1.6)%	0.6924 ± 0.0068 (2.8 ± 1.0)%	144.3 ± 0.8 (-1.9 ± 0.5)%

Table 4: Cosmological constraints (1σ C.L.) on the parameters in different models. We define five benchmark models (BMs) in terms of v/v_0 and ω_b as the inputs. Their values are chosen to be fixed for BM_{1,2,3}, and BBN-favored (Eq. (2.4) and Eq. (2.5)) for BM_{BBN} and BM_{BBN(NL)}. We also incorporate the results of P18 and CMB+BAO/ Λ CDM+ m_e from [19]. The first one serves as the reference for demonstrating the impacts of δv_{rec} on the CMB physics, while the second one is used for their consistency check. In each box of these analyses (except for P18 ones), the first line shows the favored parameter value, and the second line shows its relative shift to the reference point.

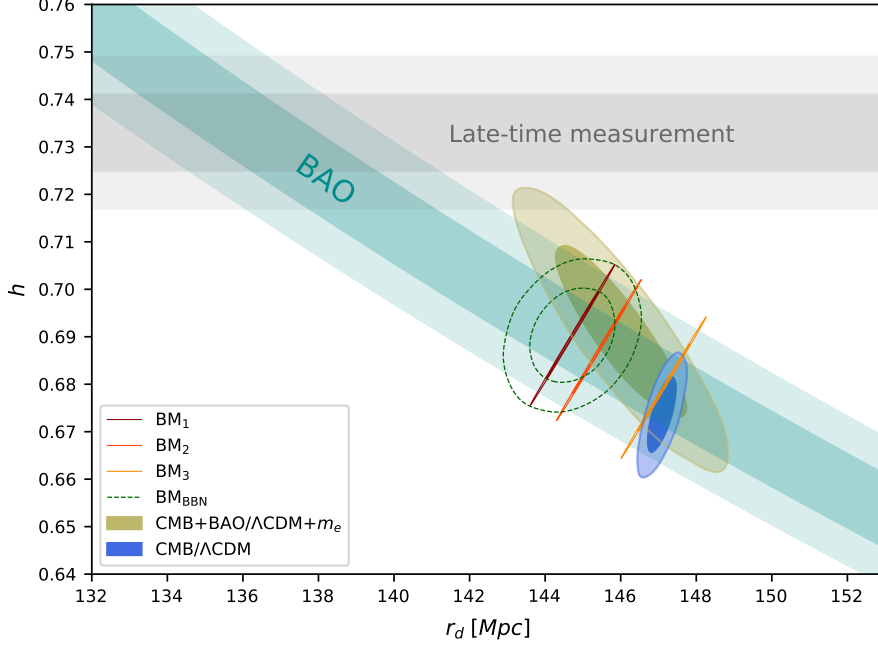


Figure 3: Cosmological constraints on r_d and h in different models. The late-time measurement of $H_0 = 73.3 \pm 0.8$ km/s/Mpc is taken from [3], while the combined BAO constraint of $r_d h = 99.95 \pm 1.20$ is from [29]. The shaded blue and khaki regions are extracted from the MCMC chains publicly by Planck team [2] and privately provided by Hart & Chluba [19], respectively. The BMs are defined in the caption of Tab. 4.

for the BMs and the CMB+BAO/ Λ CDM+ m_e analysis [19], regardless of the difference existing in their analysis methods. In [19], the relevant parameters are allowed to freely vary to fit CMB and BAO data. In our analysis, we emphasize that the two parameters, namely δv_{rec} and ω_b , are treated as inputs from BBN, while the others are determined analytically. The uncertainties for the BMs thus mainly arise from the BBN and BAO data. This explains why the favored r_d and h values in $\text{BM}_{1,2,3}$, (where the δv_{rec} and ω_b values are fixed) vary along the uncertainly direction of $(r_d h)_{\text{BAO}}$, and in BM_{BBN} additionally along another one determined by the BBN data. This also explains, at least partly, why the uncertainty contours extend for the CMB/ Λ CDM and CMB+BAO/ Λ CDM+ m_e , but do not for these BMs.

Our analytical approach requires less numerical efforts but still illustrates to some extent the mechanism of how the BAO data help to break the degeneracy of Λ CDM+ m_e fitted with the CMB data alone [19]. As a consistency check, we plug in the Λ CDM+ m_e model fitted with the

CMB+BAO data in [19] as the input, namely ⁵

$$\delta v = 0.0079 \pm 0.0071, \quad \delta \omega_b = 0.0076 \pm 0.0076, \quad (r_d h)_{\text{BAO}} = 100.9 \pm 1.4, \quad (3.27)$$

and find

$$\omega_c = 0.1208 \pm 0.002, \quad h = 0.691 \pm 0.013. \quad (3.28)$$

in perfect agreement with the values quoted earlier in Tab. 4. This check validates our linearization method.

In conclusion, in the paradigm where the Higgs VEV is allowed to vary by $\delta v_{\text{rec}} = \delta v_{\text{BBN}}$, the combination of the unchanged θ_* and varied $r_d h$ favors a higher value of H_0 than the prediction of standard Λ CDM. The Hubble tension is alleviated but not resolved.

3.3 Remarks

The method of linear extrapolation introduced for the CMB study is quite general. It allows us to quantitatively analyze the leading-order variations of cosmological parameters in beyond- Λ CDM models, as a prior step to the full-fledged MCMC simulations, and well-complements the analysis of real data. To apply this method, a crucial step is to introduce a set of relevant (information-rich, readily inferred from real data, and sufficiently many) cosmological/astronomical observables, either direct or derived ones, and define the reference point in the parameter space. Then the parameter variations w.r.t. the reference point will be constrained by the equations such as Eq. (3.13) which are introduced by varying these observables. In our analysis, we take θ_* and $r_d h$ to serve for this purpose.

θ_* is the angular sound horizon at z_* . As the distance measure of the CMB acoustic peaks, θ_* is probably one of the cosmological parameters which have been best measured. In contrast, $r_d h$ is derived from

$$\alpha_{\perp}(z_{\text{eff}})^{-1} \propto \frac{r_d}{D(z_{\text{eff}})}, \quad \text{with} \quad D(z_{\text{eff}}) \simeq \frac{\mathcal{D}}{h} \int_0^{z_{\text{eff}}} \frac{dz}{\sqrt{\Omega_m(1+z)^3 + 1 - \Omega_m}}. \quad (3.29)$$

Here $\alpha_{\perp}(z_{\text{eff}})^{-1}$ is the angular sound horizon at some redshift z_{eff} around the end of baryon drag epoch. In our analysis, $r_d h$ and hence Ω_m have been implicitly assumed to be pre-determined by the baseline CMB and BAO data. More generally, we can replace $r_d h$ with $\alpha_{\perp}(z_{\text{eff}})^{-1}$, yielding

$$d \ln D(z_{\text{eff}}) - d \ln r_d = d \ln \alpha_{\perp}(z_{\text{eff}}). \quad (3.30)$$

⁵We extract the samples of ω_b , $m_e/m_{e,0}$ and $r_d h$ from the corresponding **CosmoMC** chain kindly provided by the authors. Also, Hart & Chluba used a combined set of only low- z BAO data: 6dF [57] + MGS [58] + BOSS DR12 [65], which leads to a different constraint on $r_d h$ compared to Eq. (3.11).

As a test, we can apply this to the BAO data at different z_{eff} [29], including 6dF at $z_{\text{eff}} = 0.106$ [57], MGS at $z_{\text{eff}} = 0.15$ [58]⁶, LRG and ELG at $z_{\text{eff}} = 0.7, 0.77, 0.845$ [53, 54], QSO at $z_{\text{eff}} = 1.48$ [55], Ly- α at $z_{\text{eff}} = 2.33$ [56]. With $\delta v = 1\%$ and $\delta\omega_b = 0$, we find

$$\begin{aligned} H_0(z_{\text{eff}} = 0.106) &= 70.4 \pm 2.5, & H_0(z_{\text{eff}} = 0.15) &= 66.3 \pm 2.2, \\ H_0(z_{\text{eff}} = 0.7) &= 66.5 \pm 2.3, & H_0(z_{\text{eff}} = 0.77) &= 68.7 \pm 1.6, & H_0(z_{\text{eff}} = 0.845) &= 74.5 \pm 3.3, \\ H_0(z_{\text{eff}} = 1.48) &= 66.5 \pm 3.5, & H_0(z_{\text{eff}} = 2.33) &= 75.3 \pm 4.7. \end{aligned}$$

The combination of these H_0 values, weighted by their errors, eventually gives

$$H_{0,\text{com}} = 68.7 \pm 0.9 \text{ km/s/Mpc} . \quad (3.31)$$

This result shows an exceptional agreement with the central value of H_0 we have obtained in BM₂, where $(r_d h)_{\text{BAO}}$ is derived based on a combination of the BAO data sets said above (see footnote 4).

We are aware that the CMB spectrum contains more intrinsic features other than the peak spacing. As pointed out by Hu et.al in [66, 67], the angular sound horizon θ_* is just one of the four key parameters to characterize the spectrum. Another three are particle horizon at matter-radiation equality $l_{\text{eq}} \equiv k_{\text{eq}} D_*$, damping scale $l_d \equiv k_d D_*$ and baryon-photon momentum density ratio R_* . Potentially, these observables can be also incorporated into this analysis. But, developing such a comprehensive formalism is beyond the scope of this work.

4 Axi-Higgs Model

To address the ⁷Li puzzle and the Hubble tension, Higgs VEV v has to stay $\sim 1\%$ higher than its present value v_0 from the BBN epoch (~ 3 minutes after big bang) to the recombination epoch ($\sim 380,000$ years) and then drops to v_0 afterwards, which is known to be stabler than a variation of 10^{-16} per year [20, 21]. Here we will present a model of an axion coupled to the Higgs field to achieve this goal. The properties of this model help to resolve the discrepancies in the ⁷Li abundance and the Hubble tension discussed in the above sections as well as provide a natural explanation to the S_8/σ_8 tension and the ICB anomaly which will be discussed in the next sections.

When the electroweak scale v_0 and the SUSY breaking scale m_s are 100 GeV or larger, each of both (with its radiative corrections) will introduce a shift to the vacuum energy density Λ by many orders of magnitude bigger than the observed value Λ_{obs} which is exponentially small. So a fine-tuning is needed to obtain the right Λ_{obs} . To naturally generate such a Λ_{obs} , in the SUGRA model, the SUSY-breaking and the electroweak-scale contributions to Λ must shield each other

⁶Only the isotropic BAO scales, defined as $\alpha_V \propto \alpha_{\perp}^{2/3} \alpha_{\parallel}^{-1/3}$, are available for 6dF and MGS.

precisely [25]. Motivated by string theory, one can start with a SUGRA model as a low-energy effective theory. A natural SUSY breaking mechanism is to introduce anti-D3-branes [68], where m_s^4 is the warped brane tension. In the brane world scenario, the anti-D3-branes span our 3-dimensional observable universe, where all known SM particles (except the graviton) are open string modes living inside these anti-D3-branes.

In flux-compactified Calabi-Yau orientifold in Type IIB string theory, an anti-D3-brane brings in a nilpotent superfield X (i.e., $X^2 = 0$, so the scalar degree of freedom in X is absent) [69–71], to facilitate the SUSY breaking [72–74]. Applying X as a projection operator [75] to carry out the projection employed in [23], the two electroweak Higgs doublets H_u, H_d in SUGRA are reduced to a single doublet ϕ . The superpotential W contributes to the Higgs potential V_ϕ as

$$W = X(m_s^2 G(A) - \kappa K(A) H_u H_d) + \dots \rightarrow V_\phi = |m_s^2 G(a) - \kappa K(a) \phi^\dagger \phi|^2, \quad (4.1)$$

where we have introduced coupling functions $G(A)$ and $K(A)$. It has been shown that the anti-D3-branes couple to the closed string modes like complex structure moduli and dilaton [69, 70, 74, 76], collectively described here as superfield A . The coupling $G(A)$ is expected, as the warped throat in which the anti-D3-branes sit is described by the complex structure moduli and the dilaton (as well as fluxes with discrete values). Since each of these modes contains a complex scalar boson, an axion field can come from either a complex structure modulus or the dilaton, or some combination, as a partner of them. Because the Higgs fields are open string modes inside the anti-D3-branes, we expect a coupling between a and ϕ also, which is mediated by $K(a)$.

In this model, because of the perfect square form of V_ϕ in Eq. (4.1), the SUSY breaking and the Higgs contribution to the vacuum energy density are arranged to precisely cancel each other, allowing a naturally small Λ , as proposed in the Racetrack Kähler Uplift (RKU) model [24]. Here, all moduli are assumed to be stabilized except for the axion a (or multiple fields in A) and the Higgs field ϕ . For later convenience, we choose this particular form such that

$$v_0 = \frac{\sqrt{2}m_s}{\sqrt{\kappa}} = 246 \text{ GeV}, \quad m_\phi = 2\sqrt{\kappa}m_s = 125 \text{ GeV}. \quad (4.2)$$

This implies $m_s = 104.3 \text{ GeV}$ and $\kappa = 0.36$.

Since W has mass dimension three, we have, to a leading-order approximation,

$$G(a) = 1 + \frac{ga^2}{M_{\text{Pl}}^2}, \quad K(a) = 1 + \frac{ka^2}{M_{\text{Pl}}^2}, \quad (4.3)$$

where g and k are parameters of order one. We have normalized the functions $G(a)$ and $K(a)$ so that at the locally stable minimum $a = 0$, they take values $G_0 = K_0 = 1$. The axion a naturally has its scale f_a that appears as a dimensionless quantity a/f_a in the axion potential. Here we have absorbed these scales into coupling constant at the front like $g'a^2/f_a^2 = ga^2/M_{\text{Pl}}^2$. For the

sake of simplicity, we do not introduce mixing between axions. Then the total scalar potential can be expressed as

$$V = V_a + V_\phi = V_a(a) + |K(a) (m_s^2 F(a) - \kappa \phi^\dagger \phi)|^2, \quad (4.4)$$

with

$$F(a) = \frac{G(a)}{K(a)} \simeq 1 + \frac{Ca^2}{M_{\text{Pl}}^2}, \quad (4.5)$$

where $C = g - k$ is a constant whose positivity is undetermined. Then we have

$$\langle \phi^\dagger \phi \rangle = \frac{v^2}{2} = \frac{m_s^2}{\kappa} F(a). \quad (4.6)$$

Here the impact of the function $F(a)$ is screened by Higgs VEV. $K(a)$ plays no important role here, so we simply set $K(a) = 1$. If a is replaced with a scalar mode φ , we will have $F(\varphi) = 1 + d_1 \varphi / M_{\text{Pl}} + d_2 (\varphi / M_{\text{Pl}})^2 + \dots$ instead. The oscillation of δv then follows $\varphi(t)$ (instead of $\varphi(t)^2$) at leading order, and hence cannot be suppressed to a level allowed by observations today. So it is hard to find a solution, unless d_1 is fine-tuned to be negligibly small while d_2 is kept ~ 1 .

The dilaton S and the complex structure moduli U_j also enters the superpotential $W = W_0(U_j, S) + \dots$, where $V_a(a) \sim |DW|^2$, so $V_a(a)$ is proportional to a perfect square and vanishes at its minimum. As an axion enters in W as a phase, it is reasonable that $V_a(a) \sim |\sin(a/2f_a)|^2 = 1 - \cos(a/f_a)$. The evolution of a essentially depends on the form of $V_a(a)$ which is typically given by

$$V_a = m_a^2 f_a^2 \left(1 - \cos \frac{a}{f_a} \right) = \frac{1}{2} m_a^2 a^2 - \frac{m_a^2 a^4}{24 f_a^2} + \dots. \quad (4.7)$$

Here f_a appears only as a next-order effect. But, it appears in the interaction with the electromagnetic (EM) field via

$$\mathcal{L} \sim \frac{c_\gamma}{32\pi^2} \frac{a}{f_a} F_{\mu\nu} \tilde{F}^{\mu\nu} \quad (4.8)$$

where $F_{\mu\nu}$ is the EM field strength and $\tilde{F}_{\mu\nu}$ is its dual. c_γ is the parameter introduced by hand to describe physics beyond. In this article, we fix it to unity, $c_\gamma = 1$, a value usually viewed to be “natural”.

4.1 Single-Axion Model

Let us consider single-axion model first. Because of their interaction in V_ϕ (see Eq. (4.1) and Eq. (4.4)), the axion and Higgs fields evolve as a coupled system in the early universe. In general, the evolution of the heavier boson will significantly affect the evolution of the lighter one in such a system. But, this axi-Higgs model, originally motivated by string theory and the requirement of a naturally small Λ , demonstrates an opposite but desirable behavior.

With $\phi = v/\sqrt{2}$, the potential is

$$V = V_a + V_\phi \simeq \frac{m_a^2}{2} a^2 + |B(a, v)|^2 \quad (4.9)$$

where

$$B(a, v) = m_s^2 \left(1 + \frac{Ca^2}{M_{\text{Pl}}^2} \right) - \kappa \frac{v^2}{2} . \quad (4.10)$$

The equations of motion for $a(t)$ and $v(t)$ are

$$\ddot{a} + 3H\dot{a} + \left[m_a^2 + \frac{4Cm_s^2}{M_{\text{Pl}}^2} B \right] a \simeq 0 , \quad (4.11)$$

$$\ddot{v} + (3H + \Gamma_\phi) \dot{v} - 2\kappa Bv = 0 . . \quad (4.12)$$

Here the scale of $B(a, v)$ is $m_s^2 \simeq (100 \text{ GeV})^2$. At first sight, the term $4Cm_s^4/M_{\text{Pl}}^2$ is $\sim 10^{50} m_a^2$, and hence may have a huge impact on the evolution of a . Fortunately, this is not the case. Note that the minimum value $B_{\text{min}}(a, v) = 0$ happens at $v \neq 0$. Instead,

$$B(a, v + \Delta v) = B_{\text{min}}(a, v) + \left. \frac{\partial B}{\partial v} \right|_{\Delta v=0} \Delta v + \dots = -\kappa v \Delta v + \dots . \quad (4.13)$$

Therefore,

$$-2\kappa Bv = 4\kappa m_s^2 \left(1 + \frac{Ca^2}{M_{\text{Pl}}^2} \right) \Delta v + \dots . \quad (4.14)$$

Eq. (4.12) implies that ϕ (or v) would stabilize at the value that makes the last term vanish, which is $B_{\text{min}} = 0$ (also the minimum of its potential). Due to the presence of $\Gamma_\phi \simeq 4 \text{ MeV}$, this process happens rapidly. As the evolution of a is much slower, this implies that we can simply treat $B = 0$ in Eq. (4.11) for all time. In short, due to the strong dissipation caused by a large decay width $\Gamma_\phi \sim 4 \text{ MeV} \gg H(t > t_{\text{EW}})$, any deviation of the Higgs evolution from its stable point is instantly damped. Then thanks to V_ϕ 's perfect square form, the C term in Eq. (4.11) drops out. The Higgs field is thus stabilized to the axion-driven profile (see Eq. (4.6)), while the axion evolution is approximately described by the physics for a damped harmonic oscillator:

$$\ddot{a} + 3H(t)\dot{a} + \frac{\partial V_a}{\partial a} = 0 . \quad (4.15)$$

where the full cosine form of V_a Eq. (4.7) is used.

At early cosmic time, the large $H(t)$ freezes the axion field $a(t)$ to an initial value a_{ini} . This value is determined by Eq. (4.6) to be

$$a_{\text{ini}} = \left(\frac{2\delta v_{\text{ini}} M_{\text{Pl}}^2}{C} \right)^{1/2} , \quad (4.16)$$

together with an assumption of $\delta v_{\text{ini}} = \delta v_{\text{rec}} = \delta v_{\text{BBN}}$. The axion field $a(t)$ will not roll down to its potential minimum until $H(t) \lesssim m_a$. Then it starts to oscillate around the minimal point in an underdamped manner, yielding

$$a(t) \simeq \mathcal{A}_m(t) a_{\text{ini}} \cos(m_a t) . \quad (4.17)$$

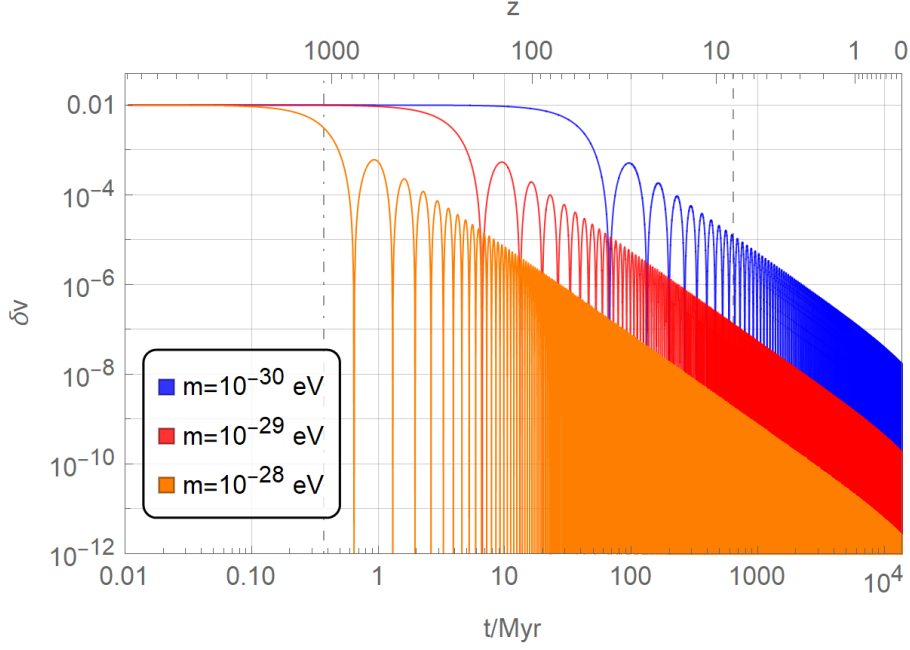


Figure 4: Cosmic evolution of the fractional deviation $\delta v = \Delta v/v_0$ of Higgs VEV, for different axion masses. The recombination time, $t_{\text{rec}} \sim 0.34$ Myrs, is labelled by the vertical dot-dashed line on the left. The redshift $z = 8$, which sets the earliest possible QS probe for δv , is labelled by a vertical dashed line on the right.

Here the oscillation period is dictated by m_a . The dimensionless amplitude $\mathcal{A}_m(t)$ decreases exponentially with a characteristic time scale $\sim H(t)^{-1}$.

In the axi-Higgs model, we are interested in the mass range such that the axion field starts to roll down near or after the recombination and oscillates with a highly-suppressed amplitude at low redshift and today. The former requirement ensures that the assumption of $\delta v_{\text{BBN}} = \delta v_{\text{rec}}$, which lays out our discussions so far, is not broken, as the Higgs VEV evolves following

$$\delta v(t) = F(a(t))^{1/2} - 1 \simeq \frac{Ca(t)^2}{2M_{\text{Pl}}^2}. \quad (4.18)$$

This sets the upper limit of m_a to be $\lesssim 3.3 \times 10^{-29}$ eV. The latter requirement ensures that this model can survive the existing constraints for the variation of Higgs VEV, from both astronomical observations, e.g., the Qs, and local laboratory experiments such as ACs [77, 78]. Given that a smaller axion mass yields a later rolling down of the axion field, which in turn yields a bigger axion amplitude and a bigger Higgs VEV oscillation amplitude today, this requirement puts a lower bound on m_a . Explicitly, the time variation of δv is given by

$$\left. \frac{d(\delta v)}{dt} \right|_{t_0} \simeq \frac{d}{dt} \left[\frac{C\mathcal{A}_{m,0}^2 a_{\text{ini}}^2 \cos^2(m_a t)}{2M_{\text{Pl}}^2} \right] = -\delta v_{\text{ini}} m_a \mathcal{A}_{m,0}^2 \sin(2m_a t), \quad (4.19)$$

where the condition that the current characteristic time scale of \mathcal{A}_m decay is much longer than m_a^{-1} is applied, and a shorthand notation of $\mathcal{A}_{m,0} = \mathcal{A}_m(t_0)$ is taken. The AC measurements [20,

21] put a strong bound on the variation rate in electron-to-proton mass ratio $\mu = m_e/m_p$, yielding $|d(\delta v)/dt|_{t_0} \lesssim 10^{-16} \text{ yr}^{-1}$. Then the lower bound on m_a can be found by marginalizing the axion oscillation phase in Eq. (4.19). Eventually, the AC measurements results in

$$m_a \in [1.0, 3.3] \times 10^{-29} \text{ eV} . \quad (4.20)$$

at 68% C.L., with the lower bound being extended to $1.6 \times 10^{-30} \text{ eV}$ at 95% C.L. Such an ultralight axion theoretically is quite acceptable in string theory [26, 27]. The variation of the Higgs VEV with $z < 8$ can be also probed by measuring the molecular absorption spectra of the QSs. The details of these analyses are presented in Sec. 8.

The cosmic evolution of $\delta v(t)$ for various axion masses is shown in Fig. 4. As expected, $\delta v(t)$ starts to roll down before the recombination for $m_a \sim 10^{-28} \text{ eV}$, yielding a δv_{rec} too small to help in resolving the Hubble tension. In contrast, for $m_a \sim 10^{-30} \text{ eV}$, $\delta v(t)$ still oscillates with a relatively large amplitude at low redshift. It is ready to be confirmed or disproved at 2σ C.L. by the ongoing measurements. These tests could be extended to the scenario with $m_a \sim 10^{-29} \text{ eV}$ in the near future.

Now let us take a look how the parameters in this model are determined. We take $m_a = 10^{-29} \text{ eV}$ as the benchmark and assume $\delta v_{\text{ini}} = \delta v_{\text{BBN}}$ at the initial moment. From the ICB analysis [4, 79], the ratio between a_{ini} and f_a is determined by (β is defined in Sec. 7)

$$\frac{a_{\text{ini}}}{f_a} = 16\pi^2\beta \simeq 0.97 . \quad (4.21)$$

Assuming that this axion contributes a small fraction x of total matter density today, we have

$$\left(\frac{1}{1+z_a}\right)^3 m_a^2 f_a^2 \left(1 - \cos \frac{a_{\text{ini}}}{f_a}\right) \simeq \omega_a (0.0030 \text{ eV})^4 . \quad (4.22)$$

Here ω_a is the axion physical density and z_a is the redshift when this axion field starts to roll down. Explicitly, z_a solves the equation $\xi H(z_a) = m_a$, with $1 \leq \xi \leq 3$. We are talking about the matter-dominated epoch, where $H(z) \propto (1+z)^{3/2}$, so we have $(1+z_a) \propto m_a^{2/3}$. This means that z_a and m_a essentially have no impacts on f_a and a_{ini} due to a cancellation, eventually yielding

$$\begin{aligned} a_{\text{ini}} &\simeq 3.7 \times 10^{17} \text{ GeV} \left(\frac{x}{0.01}\right)^{1/2} \left(\frac{\xi}{1.5}\right)^{-1} , \\ f_a &\simeq 3.8 \times 10^{17} \text{ GeV} \left(\frac{x}{0.01}\right)^{1/2} \left(\frac{\xi}{1.5}\right)^{-1} . \end{aligned} \quad (4.23)$$

According to Eq. (4.16), one finds

$$C \simeq 0.84 \left(\frac{\delta v_{\text{ini}}}{0.01}\right) \left(\frac{x}{0.01}\right)^{-1} \left(\frac{\xi}{1.5}\right)^2 . \quad (4.24)$$

We have four parameters in this single-axion model: m_a , δv_{ini} , a_{ini} , f_a . The amazing thing is that they are all reasonably constrained (see Fig. 1). $\delta v_{\text{ini}} = \delta v_{\text{BBN}} = \delta v_{\text{rec}}$ is imposed to resolve

the BBN and Hubble tensions. The ICB measurement puts constraint on a_{ini}/f_a . Together with the constraint from S_8/σ_8 , we obtain the values of a_{ini} and hence of f_a . If the fraction x is too small, the coupling constant C in Eq. (4.24) would be unreasonably large. Therefore, the parameters of this model are well-determined.

4.2 Two-Axion Model

In the single-axion model, $\delta v(t)$ drops over time. So the Higgs VEV at the BBN epoch is larger than that at the recombination time, *i.e.*, $\delta v_{\text{BBN}} \gtrsim \delta v_{\text{rec}}$. But, according to the discussions above, a δv_{rec} bigger than 1.1%, namely the value favored by the BBN, may address better the Hubble tension. We argue that this behavior could be achieved with the introduction of a second axion.

In fact, in the FDM scenario [26, 34–36], an axion with mass $\sim 10^{-22}$ eV as CDM can resolve galactic small-scale problems which are challenging the paradigm of weakly interacting massive particle. Thus we are naturally led to consider a model with two axions, denoted as a_1 and a_2 : one with a mass $m_1 \simeq 10^{-29}$ eV (here, m_1 can be relaxed from the mass range given in Eq. (4.20)) responsible for $\delta v_{\text{rec}} > 0$ and another one with a mass $m_2 \simeq 10^{-22}$ eV serving as FDM, extending $F(a)$ in Eq. (4.5) to

$$F(a_1, a_2) = 1 + \frac{C_1 a_1^2}{M_{\text{Pl}}^2} + \frac{C_2 a_2^2}{M_{\text{Pl}}^2} \quad (4.25)$$

together with a corresponding potential $V(a_2)$ for a_2 . The formula for $\delta v(t)$ is then extended by including one more axion in the function F . To the leading order, it is given by

$$\delta v(t) = F(a_1, a_2)^{1/2} - 1 \simeq \frac{C_1 a_1^2}{2M_{\text{Pl}}^2} + \frac{C_2 a_2^2}{2M_{\text{Pl}}^2}. \quad (4.26)$$

The contributions of a_1 and a_2 to total matter density today, *i.e.*, $x_{1,2} = \frac{\omega_{1,2}}{\omega_m}$, are related by $x_2 \sim 100x_1$. Here the mixing between these two axions has been neglected. To study how a_1 and a_2 evolve, we simply assume the potential of a_2 to be $V_2 \approx \frac{1}{2}m_2^2 a_2^2$ and take a value of 1.5 for ξ . Here, a_2 starts at $a_2 = a_{2,\text{ini}}$ and begins to roll down at a redshift $z_{\text{rec}} \ll z_2 \simeq 2.0 \times 10^6 \ll z_{\text{BBN}}$, where the universe is still dominated by radiation. While applying Eq. (4.22) to derive $a_{2,\text{ini}}$, note that no cancellation happens between the $(1+z_2)^{-3}$ and m_2^2 factors. We find (with Eq. (4.23))

$$a_{1,\text{ini}} \simeq 3.7 \times 10^{17} \text{ GeV}, \quad a_{2,\text{ini}} \simeq 1.5 \times 10^{17} \text{ GeV}. \quad (4.27)$$

The fact that $a_{1,\text{ini}}$ and $a_{2,\text{ini}}$ are comparable indicates that both can be important in $F(a_1, a_2)$. At $z_{\text{BBN}} \sim 10^9$, if we have $C_1 C_2 < 0$, the contributions of a_1 and a_2 to δv_{BBN} can be cancelled to some extent. At z_{rec} , since the oscillation amplitude for a_2 is already highly suppressed, δv_{rec}

will be determined by a_1 only. A scenario with $\delta v_{\text{rec}} > \delta v_{\text{ini}} = \delta v_{\text{BBN}}$ thus can be easily achieved. Explicitly, by solving

$$\frac{C_1 a_{1,\text{ini}}^2}{2M_{\text{Pl}}^2} + \frac{C_2 a_{2,\text{ini}}^2}{2M_{\text{Pl}}^2} = \delta v_{\text{BBN}}, \quad \frac{C_1 a_1^2(t_{\text{rec}})}{2M_{\text{Pl}}^2} = \delta v_{\text{rec}}. \quad (4.28)$$

For example, for $\delta v_{\text{BBN}} = \delta v_{\text{ini}} = 1\%$ and $\delta v_{\text{rec}} = 2\%$,

$$C_1 \simeq 1.7, \quad C_2 \simeq -5.1, \quad (4.29)$$

a scenario more favored in addressing the Hubble tension. Here C_1 and C_2 are of the same order and hence no fine-tuning is involved.

In summary, the FDM axion, namely a_2 with $m_2 \sim 10^{-22}$ eV and $\omega_2 = \omega_c$, can be easily incorporated into the axi-Higgs model. We can choose the 5 parameters: $m_1 \simeq m_a$, $f_1 \simeq f_a$, δv_{BBN} , δv_{rec} and x (or ω_a) to fix the model. Thus, with one extra parameter beyond the single axion model, the Hubble tension could be better addressed.

Remarks

So far, we have not mentioned the Kähler modulus $T = t + i\tau$. Its inclusion will change $K(a) \rightarrow K(a, t, \tau)$ in V_ϕ in Eq. (4.4) but it does not come into $F(a)$ [23, 25], so our axi-Higgs model is not affected. To be specific, let us go to the RKU model [24, 25]. There, when one scan over the string landscape, the probability distribution for Λ peaks sharply at $\Lambda = 0$, so one can obtain a naturally small Λ . Matching it to the observed Λ_{obs} , one finds that $m_t \sim m_\tau \sim 10^{-33}$ eV. For $m \lesssim 10^{-33}$ eV $\sim H_0$, the field has not yet or just starts to roll down, so it may contribute more to the dark energy than to the dark matter today. The undissipated vacuum energy may dictate the cosmic acceleration today, as in the ‘‘quintessence’’ mechanism.

It is interesting to note that, the superpotential takes the form

$$W = X(m_s^2 G(A) - \kappa K(A) H_u H_d) + \mu H_u H_d + \dots$$

Although the μ term does not appear in V_ϕ in leading order [23], it does help to determine the magnitude of W [80], which leads to

$$\Lambda_{\text{obs}} = 10^{-120} M_{\text{Pl}}^4 \rightarrow \mu v^2 \sim (100 \text{ GeV})^3$$

so the electroweak scale emerges naturally without fine-tuning.

5 S_8/σ_8 Tension

The matter clustering amplitude σ_8 is the root mean square of matter density fluctuations on the scale of $R_8 = 8h^{-1}\text{Mpc}$. Intuitively, a sphere with a radius R_8 encloses a mass $\sim 10^{14}h^{-1}M_\odot$,

a typical value for galactic clusters. In the Fourier momentum space, σ_8 is defined as

$$\sigma_8^2 = \sigma^2(r = R_8) = \int_0^\infty \mathcal{P}_m(k) W^2(kR_8) dk , \quad (5.1)$$

with $W^2(kr)$ being a window function to exclude the contributions from the scales away from r .

Similar to many other cosmological parameters, σ_8 can be constrained by both lensing and the CMB measuring. Yet, the effect of σ_8 is generically inseparable from the growth rate of structure, in the galaxy-clustering observations. The direct observable is instead

$$S_8 \equiv \sigma_8 \left(\frac{\Omega_m}{0.3} \right)^\gamma , \quad (5.2)$$

which can be measured by counting the number of galaxies in terms of their redshift coordinate or via weak lensing. Here the power-law index γ depends on the observed redshift and the details of the gravity model. Conventionally, for the low-redshift universe and in the Newtonian limit, its value is fixed to $\gamma = 0.5$.

The so-called S_8/σ_8 tension [7, 82] arises from a $\sim 2 - 3\sigma$ discrepancy between the inferred S_8 value from the CMB data assuming the Λ CDM model [2]

$$S_{8,\text{CMB}} = 0.832 \pm 0.013 , \quad (5.3)$$

and its value obtained from direct measurements in the late-time universe, in particular, Dark Energy Survey (DES) [5] and Kilo-Degree Survey (KiDS-1000) [81] ⁷:

$$S_{8,\text{DES}} = 0.773_{-0.020}^{+0.026} , \quad S_{8,\text{KiDS-1000}} = 0.766_{-0.014}^{+0.020} . \quad (5.4)$$

Below, we will examine how this discrepancy can be addressed in the axi-Higgs model, using

$$S_{8,\text{P18}} = 0.8325 \quad (5.5)$$

as the reference point for our linear extrapolation.

To extract out the S_8 physics in the axi-Higgs model with an additional axion of mass $\sim 10^{-29}$ eV, let us start with its variation

$$\delta S_8 = 0.5 \delta \Omega_m + \delta \sigma_8 . \quad (5.6)$$

With the relation $\Omega_m \equiv (\omega_b + \omega_c + \omega_a + \omega_\nu)/h^2$, the calculation of $\delta \Omega_m$ is straightforward, yielding

$$\delta \Omega_m = \frac{\omega_b}{\omega_m} \delta \omega_b + \frac{\omega_c}{\omega_m} \delta \omega_c + x - 2\delta h . \quad (5.7)$$

⁷The late-time value for S_8 reported by DES is a combined constraint utilizing a variety of independent measurements, mostly relying on weak lensing. In fact, these weak lensing based measurements are consistent with other late-time measurements of cluster abundance [5, 6, 83]. All the late-time measurements consistently converge on the late-time value for S_8 , and thus the discrepancy between the early time and the late-time measurements is less probably induced by calibration error only.

In Λ CDM, ω_ν is often fixed to be its lower bound set by neutrino oscillation experiments, thus we do not vary ω_ν here. The shift of $\delta v_{\text{rec}} \neq 0$ also impacts on S_8 via σ_8 . Using the numerical Boltzmann solver code **axionCAMB** [84, 85], we approximately find

$$\begin{aligned}\delta\sigma_8 &= \sigma_{8|b}\delta\omega_b + \sigma_{8|c}\delta\omega_c + \sigma_{8|h}\delta h + \frac{\partial \ln \sigma_8}{\partial x}x \\ &\simeq -0.179\delta\omega_b + 0.635\delta\omega_c + 0.232\delta h - 3.22x .\end{aligned}\tag{5.8}$$

$\sigma_{8|v}$ is tiny and hence has been neglected⁸. Then with (the counterparts of Eq. (3.21) and (3.22) in this context, with $\partial \ln \theta_*/\partial x = 0.3905$ and $\partial \ln r_d/\partial x \simeq 0$)

$$\delta\omega_c = 3.484\delta v_{\text{rec}} + 0.138\delta\omega_b - 1.193\delta(r_d h) - 2.409x ,\tag{5.9}$$

$$\delta h = 1.367\delta v_{\text{rec}} + 0.198\delta\omega_b + 0.743\delta(r_d h) - 0.519x ,\tag{5.10}$$

we eventually find

$$\delta\sigma_8 = -0.0454\delta\omega_b - 0.585\delta(r_d h) + 2.53\delta v_{\text{rec}} - 4.87x ,\tag{5.11}$$

$$\begin{aligned}\delta S_8 &= -0.101\delta\omega_b + 1.05\delta\omega_c - 0.768\delta h - 2.72x , \\ &= -0.108\delta\omega_b - 1.83\delta(r_d h) + 2.62\delta v_{\text{rec}} - 4.86x .\end{aligned}\tag{5.12}$$

For the four variables in this formula, $\delta(r_d h)$ is determined by data while $\delta\omega_b$ and δv_{rec} have a coefficient either too small to be useful or with a wrong sign for obtaining a negative δS_8 . Differently, the coefficient of x has a relatively big magnitude, with the right sign. The chance to resolve the S_8/σ_8 tension thus arises from x , the matter density of the axion.

In the axi-Higgs model, this axion is ultralight. Due to its wavy nature, this axion field can scale-dependently suppress structure formation in the universe. Here the suppression scale is determined by its mass m_a , while the suppression strength is determined by its matter density x . This impact has been verified by various theoretical considerations [87] and numerical work [88], despite that most existing work focuses on an axion field with $m_a \approx 10^{-22}$ eV. As discussed in detail in [86, 88], the density fluctuations of such an axion field and the CDM evolve as a coupled system in this context. Particularly, the axion quantum pressure and its potential force jointly defines a z -dependent Jeans scale

$$k_J(z) = \frac{\sqrt{m_a H(z)}}{(1+z)}\tag{5.13}$$

for the density perturbation evolution, with $k_J(z_0) \approx 7.4k_J(z_{\text{eq}}) = 0.015 \text{ Mpc}^{-1}$ for $m_a = 10^{-29}$ eV. Here $z_0 \equiv 0$ denotes the redshift today. The CDM and hence baryon fluctuations would feel this scale-dependent impact, yielding k -dependent growing paths. For the modes with

⁸We take a check indirectly using the MCMC chain from [19], and find $\sigma_{8|v} \sim \mathcal{O}(10^{-3})$. The other derivatives are calculated using numerical differentiation as shown in Appendix A.

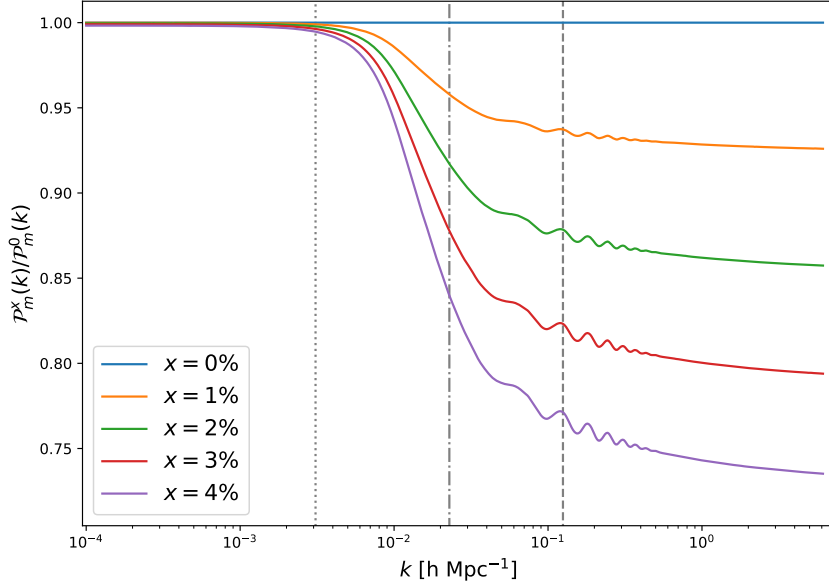


Figure 5: Suppression of the matter power spectrum for $m_a = 10^{-29}$ eV and different x values (replotting of Fig. 7 in [86], with different m_a). Here the dotted, dot-dashed and dashed vertical lines represent $k_J(z_{\text{eq}})$, $k_J(z_0)$ and $k(R_8)$, respectively.

$k < k_J(z_{\text{eq}})$ and $k > k_J(z_0)$, they stay super-Jeans and sub-Jeans respectively throughout the matter-dominated epoch. One grows while another one is suppressed. As for the modes with $k_J(z_{\text{eq}}) < k < k_J(z_0)$, they do not grow until they cross the axion Jeans scale at some moment z_k with $0 < z_k < z_{\text{eq}}$. Then under the assumption of the aligned total matter and CDM perturbations, one finds that the matter power spectrum grows as [86]

$$\frac{\mathcal{P}_m^x(k)}{\mathcal{P}_m^0(k)} = \begin{cases} 1 & \text{for } k < k_J(z_{\text{eq}}) , \\ \left(\frac{k_J(z_{\text{eq}})}{k}\right)^{10-2\sqrt{25-24x}} & \text{for } k_J(z_{\text{eq}}) < k < k_J(z_0) , \\ \left(\frac{k_J(z_{\text{eq}})}{k_J(z_0)}\right)^{10-2\sqrt{25-24x}} & \text{for } k > k_J(z_0) . \end{cases} \quad (5.14)$$

We demonstrate the suppression of the matter power spectrum for $m_a = 10^{-29}$ eV and different axion fractions x Fig. 5. Indeed, the super-Jeans modes throughout the matter-dominated epoch are not suppressed. The modes with $k_J(z_{\text{eq}}) < k < k_J(z_0)$ are suppressed to some extent which depends on when they cross the axion Jeans scale. As for the sub-Jeans modes today, to which the σ_8 mode belongs, are suppressed most. Given

$$\sigma_8 \propto \mathcal{P}_m(k(R_8))^{1/2} \quad \Rightarrow \quad \delta\sigma_8 = \left(\frac{\mathcal{P}_m^x(k)}{\mathcal{P}_m^0(k)}\right)^{1/2} - 1 , \quad (5.15)$$

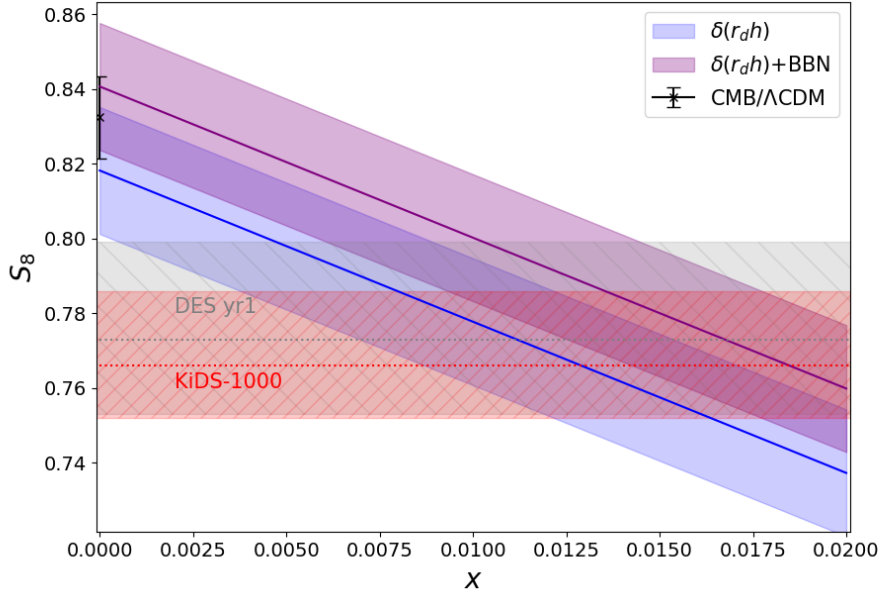


Figure 6: Dependence of S_8 on x in the axi-Higgs model. The CMB favored value in the Λ CDM model is displayed as an error bar. $\delta(r_d h)$ is turned on for both blue and purple bands. But, δx_{rec} and $\delta\omega_b$ are set to zero in the former case while the BBN inputs for them are applied in the latter one. The grey horizontal band is from DES [5] and the orange band is from KiDS-1000 [81]. All uncertainties are shown at 1σ C.L.

the dependence of σ_8 on x can be calculated straightforwardly, given by

$$\frac{\partial \ln \sigma_8}{\partial x} = \frac{24}{\sqrt{25-24x}} \left(\frac{k_J(z_{\text{eq}})}{k_J(z_0)} \right)^{10-2\sqrt{25-24x}} \ln \left(\frac{k_J(z_{\text{eq}})}{k_J(z_0)} \right) = -4.8 + \mathcal{O}(x). \quad (5.16)$$

This outcome is consistent with the result obtained from linear extrapolation in Eq. (5.11).

As $\sigma_{8||v}$ (total variation of σ_8 w.r.t cosmological parameters except for x for each percent of δv), arises from the base of the last-row quantity in Eq. (5.14) while $\frac{\partial \ln \sigma_8}{\partial x}$ is generated by some term with a big coefficient in its power, one would expect σ_8 to be more sensitive to an explicit x dependence and hence $|\frac{\partial \ln \sigma_8}{\partial x}| \gg |\sigma_{8||v}|$. This analytically-derived value of $\partial \ln \sigma_8 / \partial x$ is partly justified by our numerical calculations from Eq. (5.8), and strongly indicates that x may play a crucial role in solving the S_8/σ_8 tension.

Finally, we show the dependence of S_8 on x in the axi-Higgs model in Fig. 6. The blue and purple bands are slightly different in their heights. But in general, an x value $\sim 1-2\%$ will greatly mitigate the tension, suppressing the discrepancy from $\sim 2-3\sigma$ to $< 1\sigma$. The request of addressing this tension will eventually fix x and hence determine the values of a_{init} and f_a via Eq. (4.23).

6 Hubble Tension versus S_8/σ_8 Tension

In Sec. 2 and 3, we take an uplift for the Higgs VEV, namely $\delta v_{\text{BBN}} = \delta v_{\text{rec}} > 0$, to explore its impacts on BBN and the H_0 value, while in the previous section we introduce the axion ($m_a \sim 10^{-29}$ eV) with a matter density ω_a to study its effect on S_8/σ_8 . A priori, δv and ω_a are independent effects. In the axi-Higgs model, they are intimately connected. Here, we would like to discuss the intriguing feature how the H_0 tension and the S_8/σ_8 tension are correlated through a combination of δv and ω_a .

We have demonstrated how $\delta v_{\text{rec}} > 0$ can reduce the Hubble tension. Turning on δv_{rec} alone however exacerbates the S_8/σ_8 tension, as shown in Fig. 6. Similarly, the S_8/σ_8 tension is largely resolved by introducing axion matter abundance with $x \sim 1\%$. But, it slightly downgrades the H_0 value, as indicated in [85]. So there exists some trade off in addressing these two problems in the axi-Higgs model. The analysis in Sec. 3 focuses on $\delta v_{\text{rec}} \simeq \delta v_{\text{BBN}}$, here we will extend the analysis to allow $\delta v_{\text{rec}} > \delta v_{\text{BBN}}$.

In the single-axion model, $\delta v_{\text{BBN}} = \delta v_{\text{rec}}$, and $\delta\omega_b$ is fixed by $\delta\omega_b = 1.53\delta v_{\text{BBN}}$. However, in the two-axion model, δv_{rec} is decoupled from δv_{BBN} , where we trade the two coefficients C_1 and C_2 in $F(a_1, a_2)$ (see Eq. (4.26)) for δv_{rec} and δv_{BBN} . So we are free to vary δv_{rec} to a larger value to fit the data, while maintaining $\delta v_{\text{BBN}} = 1.1\%$. The resulting scaling of H_0 and S_8 then reads:

$$H_0 \simeq H_{0,\text{P18}} (1.01 \pm 0.01 + 1.37\delta v_{\text{rec}} - 0.52x) , \quad (6.1)$$

$$S_8 \simeq S_{8,\text{P18}} (0.98 \pm 0.02 + 2.62\delta v_{\text{rec}} - 4.86x) , \quad (6.2)$$

with the inputs of $\delta\omega_b$ from BBN and $\delta(r_{dh}) \simeq (0.9 \pm 1.2)\%$ from Eq. (3.11). The signs of the δv_{rec} and x terms in these two equations manifest the trade-off effect said above.

Model	x	δv_{rec}	ω_b	Ω_m	h	σ_8	S_8
Ref	0%	0%	0.02238	0.3158	0.6732	0.8114	0.8325
BM ₄				0.3094 ± 0.0086	0.6771 ± 0.0055	0.8076 ± 0.0052	0.8204 ± 0.0166
BM ₅	1%	$(1.1 \pm 0.1)\%$	0.02276	0.3123 ± 0.0086	0.6737 ± 0.0055	0.7681 ± 0.0052	0.7795 ± 0.0166
BM _{BBN} ⁰	0%			0.3083 ± 0.0087	0.6903 ± 0.0058	0.8289 ± 0.0057	0.8430 ± 0.0169
BM _{BBN} ^x	1%	4%	± 0.00030	0.3083 ± 0.0087	0.6868 ± 0.0058	0.7893 ± 0.0057	0.7999 ± 0.0169
BM ₆	2%			0.3100 ± 0.0087	0.7099 ± 0.0058	0.8093 ± 0.0057	0.8232 ± 0.0169
BM ₆ ^{HC}	2%	4%	± 0.00030	0.3089 ± 0.0110	0.7108 ± 0.0072	0.8086 ± 0.0067	0.8203 ± 0.0212

Table 5: S_8/σ_8 values in the axi-Higgs model. Here $\delta(r_{dh})$ is turned on for all BMs w.r.t. the reference point. Except BM₆^{HC}, where $\delta(r_{dh}) = (1.1 \pm 1.4)\%$ from [19] is applied, all BMs assume $\delta(r_{dh}) \simeq (0.9 \pm 1.2)\%$ given by Eq. (3.11). BM_{BBN}⁰ and BM_{BBN}^x take inputs for δv_{rec} and ω_b from the BBN data fitting, while BM₆ and BM₆^{HC} are motivated by the two-axion model.

The correlated impacts of δv_{rec} and x on H_0 and S_8 are demonstrated in Fig. 7 (also see Tab. 5). By varying their values, we can see how the H_0 and S_8 tensions could get resolved. In

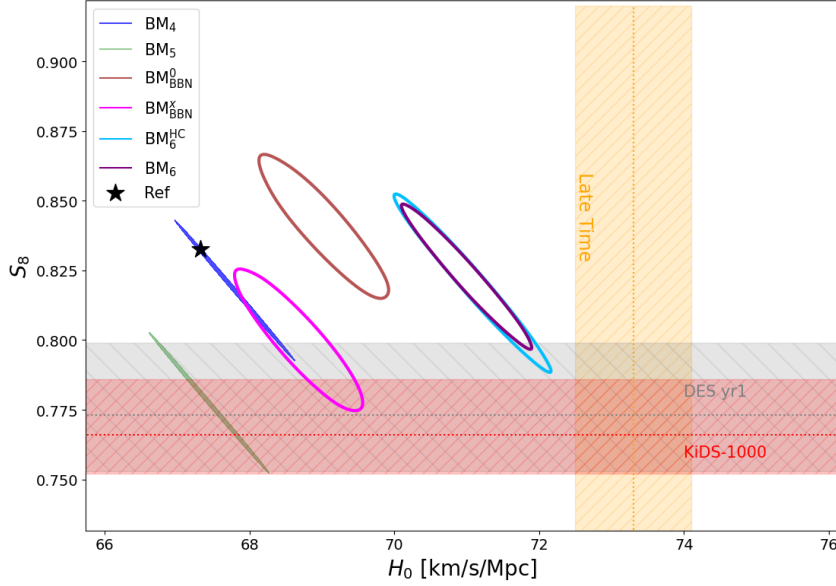


Figure 7: Correlated impacts of δv_{rec} and x on H_0 and S_8 . The orange band is the late-time determination of H_0 [3]. The grey and red bands denote the S_8 values from DES [5] and KiDS-1000 [81], respectively. The BMs are defined in Tab. 5. All uncertainties are shown at 1σ C.L.

this figure, the circles are all stretched from left-upper to right-bottom, by the uncertainty of $\delta(r_d h)$. According to Eq. (5.10) and Eq. (5.12), a bigger $r_d h$ value increases the H_0 value and decreases the S_8 value, and hence reduces both Hubble and S_8 tensions from the data side. In terms of the parameters in the axi-Higgs model, *i.e.*, δv_{rec} and x , their impacts are demonstrated using a set of BMs. BM_5 and BM_{BBN}^0 represent the scenarios where one of them is turned on. They are shifted away from BM_4 , where $\delta v_{\text{rec}} = x = 0$, along the direction from left-bottom to right-upper or its opposite. This feature reflects the said trade-off effect. But, one can see that BM_{BBN}^x does bring the favored value toward the intersection region of the late time (vertical) band and the S_8 (horizontal) bands. Hence both H_0 and S_8 tensions get alleviated to some extent. Yet, the choice of

$$\delta v_{\text{rec}} \simeq 4\%, \quad x \simeq 2\%, \quad (6.3)$$

namely BM_6 and BM_6^{HC} (characterized by different $r_d h$ values from BAO) which are motivated by the two-axion model, results in a slight overlap between them.

Notably, turning on x or the axion matter density can have non-trivial impacts on the CMB data fitting. While incorporating the axion in ΛCDM , ref. [85] finds that x is limited to $\lesssim (2.2 - 3.0)\%$ for $m_a \sim 10^{-30} - 10^{-29}$ eV at 95% C.L. This indicates that the two-axion model may better resolve the Hubble and $S_8(\sigma_8)$ tensions. Yet, as $\delta v \equiv 0$ in [85], a full-data analysis in the axi-Higgs model with $\delta v \neq 0$ and $x \neq 0$ is required before stronger statements can be made.

7 Isotropic Cosmic Birefringence

Most of the ongoing or proposed axion detections are based on the axionic Chern-Simon interaction with photons defined in Eq. (4.8). The magnitude of their coupling g is model-dependent. This interaction violates parity in an axion background, correcting dispersion relation differently for left- and right-circularly-polarized photons. It thus yields an effect of cosmic birefringence when photons, if being linearly polarized, travel over an axion background in the universe [30–32].

Cosmic birefringence opens an avenue to explore axion physics. In last decades a series of cosmological and astrophysical observations such as CMB [32, 89, 90], radio galaxy and active galactic nucleus [30, 91], pulsar [92, 93], protoplanetary disk [94], blackhole [95], etc. have been proposed to detect this effect. Recently, by reanalyzing P18 polarization data with an improved estimation on miscalibration in the polarization angle at its detectors, the authors of [4] report that an ICB effect in the CMB, namely $\beta = 0.35 \pm 0.14$ deg, has been observed with a statistical significance of 2.4σ . Here β is the net rotation made by cosmic birefringence in the linear polarization angle of CMB. If being confirmed later, this observation will be an unambiguous evidence for physics beyond the SM.

This ICB analysis is based on the C_ℓ^{EB} spectrum, a CMB observable known to be sensitive to parity-violating physics [90]. Cosmic birefringence rotates the linear polarization of the CMB photons by an angle [32]

$$\beta = \frac{1}{16\pi^2 f_a} \int_{t_{\text{LSS}}}^{t_0} dt \dot{a} = \frac{1}{16\pi^2 f_a} \left[a(t_0) - a(t_{\text{LSS}}) \right], \quad (7.1)$$

and yields a contribution, namely

$$C_\ell^{EB, \text{obs}} = \frac{1}{2} \sin(4\beta) (C_\ell^{EE} - C_\ell^{BB}), \quad (7.2)$$

to the C_ℓ^{EB} spectrum observed today [90, 96, 97]. Here C_ℓ^{EE} and C_ℓ^{BB} are the intrinsic EE and BB spectra at last scattering surface (LSS). $a(t_0)$ and $a(t_{\text{LSS}})$ represent the axion profiles at present and LSS. Their fluctuations, which are anisotropic and hence not relevant here, have been left out. Generally, the calculation of β in statistics is involved, as the value of $a(t_{\text{LSS}})$ for the CMB photons may vary a lot. But, for $H_0 \lesssim m_a \lesssim H(t_{\text{LSS}})$, the scenario that we are interested in, the axion field starts to roll down and oscillate after the last scattering of the CMB photons. $a(t_{\text{LSS}})$ thus can be naturally approximated as a constant, *i.e.*, a_{ini} , for all CMB photons. Eq. (7.1) is then reduced to

$$\beta \sim -\frac{1}{16\pi^2} \frac{a_{\text{ini}}}{f_a}, \quad \Rightarrow \quad \frac{a_{\text{ini}}}{f_a} \simeq 1.0 \pm 0.3. \quad (7.3)$$

Note that a minus sign has been dropped here for $\frac{a_{\text{ini}}}{f_a}$ for convenience (see footnote 2).

Now we are able to draw an overall picture on the axi-Higgs cosmology in the single axion version of the model. (Note that, with $m_2 \sim 10^{-22}$ eV in the 2-axion version, the a_2 oscillation is rapid during recombination time so the time averaging of its fast oscillation renders

negligible its contribution to ICB.) As discussed in Sec. 4, this axi-Higgs model is parametrized by four free parameters. For the convenience of presentation, we redefine $F(a)$ in Eq. (1.1) as $F(a) = 1 + C'a^2/f_a^2$, with $C' = Cf_a^2/M_{\text{Pl}}^2$, and choose them to be: m_a , C' , $\frac{a_{\text{ini}}}{f_a}$ and f_a . These parameters are then applied to address five classes of astronomical/cosmological observations and measurements then: (1) AC/QS; (2) CMB+BAO; (3) BBN; (4) S_8/σ_8 and (5) ICB. This picture is demonstrated in Fig. 1. In this figure, the right edge of the shaded green region shows the upper bound of the axion mass. It is determined by the requirement that the axion does not roll down until near or after the recombination. The lower limit of m_a is set by the AC measurement of the μ drift rate [22]. The projected lower limits from astronomical observations of molecular absorption spectra, based on the present and the two-order improved precisions for eighteen known Qs [33], are also presented. The shaded purple region represents a recast of the CMB+BAO data interpretation in $\Lambda\text{CDM}+m_e$ (previously proposed to address the Hubble tension in [19]) in this axi-Higgs model. The shaded orange region is responsible for addressing the ${}^7\text{Li}$ problem. At leading order, only $C' \left(\frac{a_{\text{ini}}}{f_a}\right)^2$ matters for both. This quantity induces the shift in the Higgs VEV, namely δv_{BBN} and δv_{rec} , according to the axion-Higgs coupling. As shown in Fig. 1, the $\frac{a_{\text{ini}}}{f_a}$ values (and hence the $C' \left(\frac{a_{\text{ini}}}{f_a}\right)^2$ values) favored by the CMB+BAO and the BBN data are fully overlapped at 1σ level! The ICB is determined by $\frac{a_{\text{ini}}}{f_a}$ only. A choice of $C' \sim \mathcal{O}(0.01)$ allows these three puzzles to be addressed simultaneously! At last, the S_8/σ_8 tension can be mitigated with a percent-level contribution from this axion to dark matter energy density. We present the f_a contours in this figure, assuming $x = 0.01$, with a_{ini} being approximately determined by

$$\frac{1}{2}m_a^2 a_{\text{ini}}^2 = x\rho_m(z_a + 1)^3 \quad . \quad (7.4)$$

Here ρ_m is the total matter energy density today. In the intersection region of all, f_a is favored to be $\sim 10^{17} - 10^{18}$ GeV. At last, it is worthwhile to point out that an axion with $m_a \sim 10^{-30} - 10^{-29}$ eV, as favored in the axi-Higgs model, falls into the ‘‘vanilla’’ region to explain this ICB anomaly. Heavier axions such as the FDM axion tend to start to oscillate earlier and hence to contribute less with a suppressed $a(t_{\text{LSS}})$ (see, e.g., [79]).

8 Testing the Axi-Higgs Model

In the axi-Higgs model, the axion (or the lighter axion in the two-axion version) rolls down near or after the recombination and oscillates with a highly-suppressed amplitude at low redshift and today. As discussed in Sec. 4, this expectation well-determines the mass range allowed for this axion. It also lays out the foundation to test this model in the near future. Here involved are the AC and QS measurements.

The AC measurements are sensitive to the temporal drift rate of $\delta v(t)$ since atomic frequen-

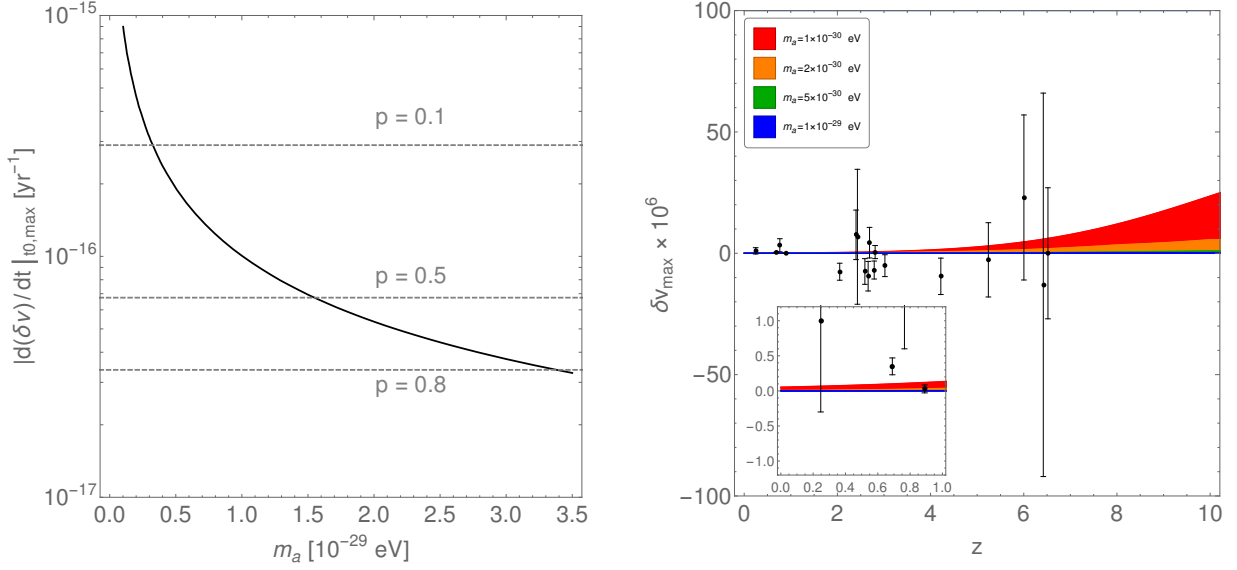


Figure 8: Late-time constraints on $\delta v(t)$. Left: Maximal drift rate $|d(\delta v)/dt|_{t_0}$ as a function of m_a , versus the p values after marginalizing the axion oscillation phase, with the AC data [22]. Right: Maximal δv as a function of z , versus the QS data at different redshifts [33]. In both panels, we take 1.1% as the δv_{ini} benchmark value.

cies depend on the parameters such as $\mu = m_e/m_p$ ⁹. By measuring the time dependence of various types of ACs, these experiments are able to limit the local drift rate $\delta v_{||t}$ to a level of $\lesssim \mathcal{O}(10^{-16}) \text{ yr}^{-1}$ [20–22]. Let us consider the latest limit reported in [22]. This measurement is based on the observation of $^{171}\text{Yb}^+$ electric quadruple/octuple frequencies for several years, yielding

$$\left. \frac{d(\delta v)}{dt} \right|_{t_0} \simeq \left. \frac{d(\delta \mu)}{dt} \right|_{t_0} = (0.08 \pm 0.36) \times 10^{-16} \text{ yr}^{-1} . \quad (8.1)$$

The nowadays maximal drift rate of δv in the axi-Higgs model is determined by the relation in Eq. (4.19). Numerically, we have

$$\delta v_{\text{max}} \simeq 1.7 \times 10^{-5} \left(\frac{\delta v_{\text{rec}}}{0.01} \right) \left(\frac{1+z}{10} \right)^3 \left(\frac{m_a}{10^{-30} \text{ eV}} \right)^{-2} , \quad (8.2)$$

and hence

$$\left. \frac{d(\delta v)}{dt} \right|_{t_0, \text{max}} \simeq 1.0 \times 10^{-15} \left(\frac{m_a}{10^{-30} \text{ eV}} \right)^{-1} \text{ yr}^{-1} . \quad (8.3)$$

Note that the local drift rate will be zero if we are sitting right on the peak or trough of the axion oscillation. Consequently, it is always possible to have a $m_a \ll 10^{-29} \text{ eV}$ by tuning the

⁹AC can also put limits on the drift rates of light quark masses. However, the corresponding sensitivities are at least one order of magnitude lower than that of μ [98].

local phase of the axion oscillation. To properly take into this effect, we marginalize the axion-oscillation phase, and present the AC constraints on m_a in the left panel of Fig. 8. At 68% C.L., we exclude the models with $m_a < 1.0 \times 10^{-30}$ eV.

The measurements of the QSs, or more accurately their molecular absorption spectra, can be applied to constrain $\delta v \simeq \delta \mu$ directly. The richness of these molecular spectra helps break the degeneracy of the line shift caused by the Higgs VEV variation δv and the redshift z . For example, the energy levels of the electronic, vibrational, and rotational modes of the molecules depend on μ as [78]:

$$E_{\text{el}} \propto \mu^0, \quad E_{\text{vib}} \propto \mu^{-0.5}, \quad E_{\text{rot}} \propto \mu^{-1}. \quad (8.4)$$

Moreover, the spectral lines from the molecular (hyper)fine structure, Λ -doubling, hindered rotation, and atomic transitions can further break this degeneracy [78]. Thus we are allowed to measure the axion oscillation amplitude in the distant past directly. The typical sensitivity of the QS measurements on δv is of order $\sim \mathcal{O}(10^{-5}) - \mathcal{O}(10^{-6})$ ¹⁰. It is limited by several factors such as Doppler noise and the background emissions [33]. Although the amplitude of δv is expected to be higher at higher z , the precisions for the QS measurements become relatively low in this case. Therefore, it is valuable to combine the measurements of the QSs at all redshifts.

We demonstrate δv_{max} as a function of z in the right panel of Fig. 8. Here the data points of the QSs are taken from [33], with their z ranging from 0.25 to 6.5¹¹. Largely due to the impacts of the data points with $z < 3$, many of which have a central value deviate from $\delta v = 0$ by more than 1σ , the full range of m_a for the axi-Higgs model is excluded at 68% C.L, after the axion-oscillation phase is marginalized. This is also true for standard Λ CDM model. At 95 % C.L., however, m_a is allowed to extend to 5.1×10^{-31} eV from above, a range broader than the AC limit at the same C.L., *i.e.*, 1.6×10^{-30} eV.

So far, our discussions focus on the single-axion model. For the two-axion model, with the additional axion a_2 being the FDM candidate ($m_2 \sim 10^{-22}$ eV), the bounds on δv_{rec} is relaxed; in particular, as discussed in Sec. 6, $\delta v_{\text{rec}} \simeq 0.03$ is most reasonable. So the resulting a_1 oscillation amplitude δv_{max} in Eq. (8.2) is enhanced for $m_1 = m_a$, yielding a stronger signal strength.

The next-generation AC technology will improve its sensitivity on frequency to a level $\sim \mathcal{O}(10^{-18})\text{yr}^{-1}$. Such developments include new methods for optical lattice clocks [100], optical clocks based on highly charged ions and hyperfine transitions [101], etc. A more challenging approach of using nuclear clocks based on long-lived, low-energy isomer $^{229\text{m}}\text{Th}$ may allow us to reach a $\sim \mathcal{O}(10^{-19})\text{yr}^{-1}$ sensitivity on frequency [102, 103]. To exclude the axi-Higgs model

¹⁰The data in [33] include additionally the contributions from some astrophysical objects other than the QSs such as the QS candidates and dusty star-forming galaxies [99]. We will tolerate the inaccuracy of using the terminology of “quasar” here, since the limits obtained for m_a in this context do not rely on the identification of these objects directly.

¹¹Different from [33], where some data points at different redshifts are averaged as one input (see Fig. 3 in [33]), we treat these data points individually while drawing the right panel of Fig. 8.

with $m_a = 3.3 \times 10^{-29}$ eV at 95% C.L., the precision of measuring $|d(\delta v)/dt|$ needs to be $\lesssim 2.2 \times 10^{-18}$ yr $^{-1}$. Such a precision can be expected for the next one or two decades, using these new technologies.

We also expect an essential improvement to the precision of measuring the molecular spectra in the near future, from both infrared and radio astronomy. In terms of the infrared observations, the upcoming Thirty Meter Telescope (TMT) [104] and James Webb Space Telescope (JWST) [105] may push up the precision by more than one order of magnitude. As for the radio astronomy, the upgraded Atacama Large Millimeter/submillimeter Array (ALMA) [106], the Five-hundred-meter Aperture Spherical Radio Telescope (FAST) [107], and the Square Kilometer Array (SKA) [108] may play a complementary role, by measuring new molecular transitions with high precision [33]. In view of the great potential of the ongoing or the near-future astronomical observations in testing the axi-Higgs model, we make a modest sensitivity projection for the m_a lower limits. To achieve that, we take the uncertainty of each QS data point in Fig. 8 as the reference precision, and assume all data points to center at $\delta v = 0$ (*i.e.*, assume all data to match with the standard Λ CDM model perfectly). This immediately yields a “projected” lower limit 3.0×10^{-31} eV at 68% C.L. for m_a . Then with an improvement in precision by two orders, which could be anticipated for the said large-scale telescopes due to the advances of the light-collecting technology and the progress on the wavelength-calibration method [109], this lower limit will increase to $\sim 3.0 \times 10^{-30}$ eV. We demonstrate these results in Fig. 1.

Remarks

Driven by the evolution of the axion field, after its condensate, $\delta v(x, t)$ oscillates in the three dimensional space of our universe with a period

$$\Delta z \simeq 0.83 \left(\frac{1+z}{10} \right)^{2.5} \left(\frac{m_a}{10^{-30} \text{ eV}} \right)^{-1} . \quad (8.5)$$

Potentially this will allow us to correlate the QS data points observed and expected to be observed (and even with the AC measurements), if their redshifts are not very small compared to 10 and the axion mass m_a is $\sim 10^{-30}$ eV. This is somewhat reminiscent of the detection of stochastic gravitational waves using pulsar timing array. In this case, there is no need to take marginalization for the δv oscillation phase at each data point, while the noise in these measurements could be largely suppressed. In particular, if any evidence on $\delta v(t) \neq 0$ or $d(\delta v)/dt \neq 0$ is found directly in the near future, such an analysis would be highly valuable for probing the evolution pattern of $\delta v(t)$ and hence its nature.

9 Conclusions

Motivated theoretically by string theory and experimentally by a series of cosmological and astronomical observations, we propose a model of an axion coupled with the Higgs field, named “axi-Higgs”, in this paper. In this model, the axion and Higgs fields evolve as a coupled system in the early universe. The perfect square form of their potential, together with the damping effect of the Higgs decay width, yields the desirable feature of the model: the evolution of the Higgs VEV is driven by the axion evolution, since before the BBN.

The axi-Higgs model is highly predictive. In the single-axion version, it is parametrized by four parameters only: m_a , δv_{ini} , a_{ini} and f_a . Amazingly they are all reasonably constrained (see Fig. 1). $\delta v_{\text{ini}} = \delta v_{\text{BBN}} = \delta v_{\text{rec}}$ is imposed to resolve the BBN and Hubble tensions. The ICB measurement puts the constraint on a_{ini}/f_a . Together with the constraint from addressing the S_8/σ_8 tension, we obtain the values of a_{ini} and hence of f_a . If the a_{ini} value is too small, a fine-tuning is needed to have the favored value for δv_{ini} (see Eq. (4.24)). Therefore, the parameters of this model are well-determined.

A priori, in solving the ${}^7\text{Li}$ puzzle, only a $\delta v_{\text{BBN}} \sim 1\%$ is enough, while the axion plays no role. In explaining the ICB anomaly, only the axion properties are relevant while the variation of the Higgs VEV plays no role. It is in tackling the Hubble and S_8/σ_8 tensions that both the axion and δv_{rec} come into play (see Eq. (6.1), Eq. (6.2) and Fig. 7). Here the axi-Higgs model, in linking them together, provides a simple framework to further explore their connections.

Comprehensive investigation on the axi-Higgs model would be highly valuable. In its two-axion version, δv_{rec} is decoupled from δv_{BBN} . We are thus allowed to freely vary δv_{rec} to a larger value to fit the CMB data, while maintaining $\delta v_{\text{BBN}} \sim 1\%$. Together with a larger contribution of the axion to the total matter density today, this leads to a better resolution to both Hubble and S_8/σ_8 tensions. But, before we are able to conclude, a full-data analysis is required.

The axi-Higgs model is accessible to the near-future measurements. The axion evolution can be approximately described by the physics for a damped oscillator. It rolls down to its potential minimum after $H(t)$ drops below m_a . Then it starts to oscillate around the minimal point in an underdamped manner. The variation of the Higgs VEV may be detected by the QS spectral measurements, while its oscillating feature may be observed in the AC measurements. With further improvements in their precisions, we should test the axi-Higgs model seriously.

Acknowledgements

We thank Luke Hart and Jens Chluba for valuable communications. This work is supported partly by the Area of Excellence under the Grant No. AoE/P-404/18-3(6) and partly by the General Research Fund under Grant No. 16305219. Both grants were issued by the Research Grants Council of Hong Kong S.A.R.

A Some Analytical Formulae

Recombination and baryon drag

Recombination are prolonged processes occurred at approximately the same epoch in the thermal history. We adopt the standard definition of this moment being the redshift where the optical depth reaches unity ¹²

$$\tau(z) = \int_0^z dz \frac{\sigma_T n_e(z)}{(1+z)H(z)}, \quad \tau(z_*) = 1, \quad (\text{A.1})$$

where $H(z)$ is given in Eq. (3.3) and the free electron fraction reads

$$n_e(z) = n_H x_e(z), \quad \text{where} \quad n_H = (1 - Y_P) \frac{\rho_{b,0}}{m_H}. \quad (\text{A.2})$$

$x_e(z)$ is called the free electron fraction which is calculated based on a specific recombination model. In this work we use the numerical code **Recfast++** [111–114] ¹³ in order to account for the variation of electron mass (equivalent to the variation of Higgs VEV). The optical depth describes the opacity of the universe seen from the present age. Alternatively, recombination can also be determined approximately by the moment corresponding to the maximum of the visibility function

$$g(z) = H(z) \frac{d\tau}{dz} e^{-\tau}, \quad g(z_*) = \text{Max}[g(z)]. \quad (\text{A.3})$$

The visibility function is Gaussian-like as seen from Fig. 9, hence peaks at its mean value. The width of this function roughly represents the thickness of photon last scattering surface.

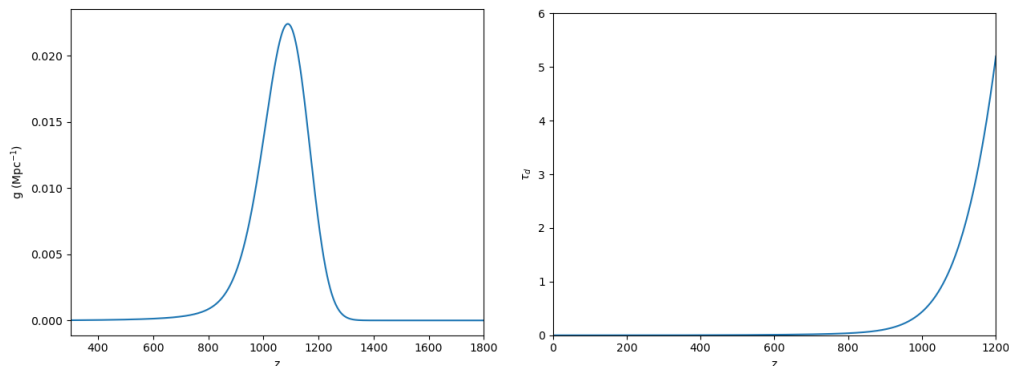


Figure 9: The visibility function and drag depth in Λ CDM.

¹²The standard definition used in **CAMB** and [110]

¹³**Recfast++** is the modified version of the original Recfast [115] with more sophisticated treatment of multi-level recombination effects, which has been studied in [116–118].

Y \ X	v/v_0	ω_b	ω_c	h
z_*	1.01845	-0.0264	0.00967	$\sim 6 \times 10^{-7}$
z_d	0.94503	0.04824	0.00823	$\sim -1 \times 10^{-7}$

Table 6: Numerical values of $Y|_X$, with $Y = z_{*,d}$.

We similarly define the drag depth and the baryon drag redshift as the moment where it reaches unity

$$\tau_d(z) = \int_0^z \frac{d\tau/dz}{R}, \quad R = \frac{3\rho_b}{4\rho_\gamma}, \quad \tau_d(z_d) = 1. \quad (\text{A.4})$$

The drag depth evolves monotonically as shown in Fig. 9. At redshifts below z_d baryon cease to being dragged by photon in their tight-coupling acoustic oscillations¹⁴. These two redshifts in our P18 reference model are precisely given by

$$z_{*,\text{P18}} = 1089.87 \quad z_{d,\text{P18}} = 1059.95. \quad (\text{A.5})$$

To compute the partial derivatives of z_* and z_d w.r.t cosmological parameters, we numerically integrate both at different using the centered second-order formula, e.g.

$$\frac{\partial \ln z_*}{\partial \ln v} = \frac{z_*(v/v_0 = 1.001) - z_*(v/v_0 = 0.999)}{0.002 z_{*,\text{P18}}}. \quad (\text{A.6})$$

The final result is given in Tab. 6, which shows the weak dependence of $z_{*/d}$ on ω_b , ω_c , h . Therefore they become insignificant in our linearization method but may play a role in higher-order corrections.

Partial derivatives

The analytical formulae used for calculating $Y|_X$ in Tab. 3 are given below, with $Y = r_{*/d}$ in the first three and $Y = D_*$ in the last three:

$$\frac{\partial \ln r_{*/d}}{\partial \ln \omega_b} = -\frac{\mathcal{D}\omega_b}{2r_{*/d}} \int_{z_{*/d}}^{\infty} dz \frac{c_s(z)}{h(z)} \left[\frac{9}{4\omega_\gamma(1+z)} + \frac{(1+z)^3 - 1}{h^2(z)} \right]; \quad (\text{A.7})$$

$$\frac{\partial \ln r_{*/d}}{\partial \ln \omega_c} = -\frac{\mathcal{D}\omega_c}{2r_{*/d}} \int_{z_{*/d}}^{\infty} dz \frac{c_s(z)}{h^3(z)} [(1+z)^3 - 1]; \quad (\text{A.8})$$

$$\frac{\partial \ln r_{*/d}}{\partial \ln h} = -\frac{\mathcal{D}h^2}{r_{*/d}} \int_{z_{*/d}}^{\infty} dz \frac{c_s(z)}{h^3(z)}; \quad \frac{\partial \ln r_{*/d}}{\partial \ln z_{*/d}} = -\mathcal{D} \frac{z_{*/d} c_s(z_{*/d})}{r_{*/d} h(z_{*/d})} \quad (\text{A.9})$$

$$\frac{\partial \ln D_*}{\partial \ln \omega_b} = -\frac{\mathcal{D}\omega_b}{2D_*} \int_0^{z_*} \frac{dz}{h^3(z)} [(1+z)^3 - 1]; \quad (\text{A.10})$$

¹⁴The value of z_d is typically taken by $r_d \simeq 1.02 r_*$ in literature for ΛCDM .

$$\frac{\partial \ln D_*}{\partial \ln \omega_c} = -\frac{\mathcal{D}\omega_c}{2D_*} \int_0^{z_*} \frac{dz}{h^3(z)} [(1+z)^3 - 1]; \quad (\text{A.11})$$

$$\frac{\partial \ln D_*}{\partial \ln h} = -\frac{\mathcal{D}h^2}{D_*} \int_0^{z_*} \frac{dz}{h^3(z)}; \quad \frac{\partial \ln D_*}{\partial \ln z_*} = \frac{\mathcal{D}z_*}{D_* h(z_*)}. \quad (\text{A.12})$$

Here $h(z) = \sqrt{\omega_r(1+z)^4 + \omega_m(1+z)^3 + \omega_\Lambda}$ is the dimensionless Hubble parameter.

References

- [1] J. P. Kneller and G. C. McLaughlin, *BBN and Lambda(QCD)*, *Phys. Rev. D* **68** (2003) 103508, [[nucl-th/0305017](#)].
- [2] **Planck** Collaboration, N. Aghanim et al., *Planck 2018 results. VI. Cosmological parameters*, *Astron. Astrophys.* **641** (2020) A6, [[arXiv:1807.06209](#)].
- [3] L. Verde, T. Treu, and A. Riess, *Tensions between the Early and the Late Universe*, *Nature Astron.* **3** (7, 2019) 891, [[arXiv:1907.10625](#)].
- [4] Y. Minami and E. Komatsu, *New Extraction of the Cosmic Birefringence from the Planck 2018 Polarization Data*, *Phys. Rev. Lett.* **125** (2020), no. 22 221301, [[arXiv:2011.11254](#)].
- [5] **DES** Collaboration, M. A. Troxel et al., *Dark Energy Survey Year 1 results: Cosmological constraints from cosmic shear*, *Phys. Rev. D* **98** (2018), no. 4 043528, [[arXiv:1708.01538](#)].
- [6] H. Hildebrandt et al., *KiDS-450: Cosmological parameter constraints from tomographic weak gravitational lensing*, *Mon. Not. Roy. Astron. Soc.* **465** (2017) 1454, [[arXiv:1606.05338](#)].
- [7] W. Handley and P. Lemos, *Quantifying tensions in cosmological parameters: Interpreting the DES evidence ratio*, *Phys. Rev. D* **100** (2019), no. 4 043504, [[arXiv:1902.04029](#)].
- [8] B. Li and M.-C. Chu, *Big bang nucleosynthesis with an evolving radion in the brane world scenario*, *Phys. Rev. D* **73** (2006) 023509, [[astro-ph/0511642](#)].
- [9] A. Coc, N. J. Nunes, K. A. Olive, J.-P. Uzan, and E. Vangioni, *Coupled Variations of Fundamental Couplings and Primordial Nucleosynthesis*, *Phys. Rev. D* **76** (2007) 023511, [[astro-ph/0610733](#)].
- [10] T. Dent, S. Stern, and C. Wetterich, *Primordial nucleosynthesis as a probe of fundamental physics parameters*, *Phys. Rev. D* **76** (2007) 063513, [[arXiv:0705.0696](#)].
- [11] T. E. Browder, T. Gershon, D. Pirjol, A. Soni, and J. Zupan, *New Physics at a Super Flavor Factory*, *Rev. Mod. Phys.* **81** (2009) 1887–1941, [[arXiv:0802.3201](#)].

- [12] P. F. Bedaque, T. Luu, and L. Platter, *Quark mass variation constraints from Big Bang nucleosynthesis*, *Phys. Rev. C* **83** (2011) 045803, [arXiv:1012.3840].
- [13] M.-K. Cheoun, T. Kajino, M. Kusakabe, and G. J. Mathews, *Time Dependent Quark Masses and Big Bang Nucleosynthesis Revisited*, *Phys. Rev. D* **84** (2011) 043001, [arXiv:1104.5547].
- [14] J. Berengut, E. Epelbaum, V. Flambaum, C. Hanhart, U.-G. Meissner, J. Nebreda, and J. Pelaez, *Varying the light quark mass: impact on the nuclear force and Big Bang nucleosynthesis*, *Phys. Rev. D* **87** (2013), no. 8 085018, [arXiv:1301.1738].
- [15] L. J. Hall, D. Pinner, and J. T. Ruderman, *The Weak Scale from BBN*, *JHEP* **12** (2014) 134, [arXiv:1409.0551].
- [16] M. Heffernan, P. Banerjee, and A. Walker-Loud, *Quantifying the sensitivity of Big Bang Nucleosynthesis to isospin breaking with input from lattice QCD*, arXiv:1706.04991.
- [17] K. Mori and M. Kusakabe, *Roles of ${}^7\text{Be}(n,p){}^7\text{Li}$ resonances in big bang nucleosynthesis with time-dependent quark mass and Li reduction by a heavy quark mass*, *Phys. Rev. D* **99** (2019), no. 8 083013, [arXiv:1901.03943].
- [18] **Planck** Collaboration, P. A. R. Ade et al., *Planck intermediate results - XXIV. Constraints on variations in fundamental constants*, *Astron. Astrophys.* **580** (2015) A22, [arXiv:1406.7482].
- [19] L. Hart and J. Chluba, *Updated fundamental constant constraints from Planck 2018 data and possible relations to the Hubble tension*, *Mon. Not. Roy. Astron. Soc.* **493** (2020), no. 3 3255–3263, [arXiv:1912.03986].
- [20] N. Huntemann, B. Lipphardt, C. Tamm, V. Gerginov, S. Weyers, and E. Peik, *Improved limit on a temporal variation of m_p/m_e from comparisons of Yb^+ and Cs atomic clocks*, *Phys. Rev. Lett.* **113** (2014), no. 21 210802, [arXiv:1407.4408].
- [21] R. M. Godun, P. B. R. Nisbet-Jones, J. M. Jones, S. A. King, L. A. M. Johnson, H. S. Margolis, K. Szymaniec, S. N. Lea, K. Bongs, and P. Gill, *Frequency Ratio of Two Optical Clock Transitions in $\text{Yb}+171$ and Constraints on the Time Variation of Fundamental Constants*, *Phys. Rev. Lett.* **113** (2014), no. 21 210801, [arXiv:1407.0164].
- [22] R. Lange, N. Huntemann, J. M. Rahm, C. Sanner, H. Shao, B. Lipphardt, C. Tamm, S. Weyers, and E. Peik, *Improved limits for violations of local position invariance from atomic clock comparisons*, *Phys. Rev. Lett.* **126** (2021), no. 1 011102, [arXiv:2010.06620].
- [23] S. Y. Li, Y.-C. Qiu, and S.-H. H. Tye, *Standard Model from A Supergravity Model with a Naturally Small Cosmological Constant*, arXiv:2010.10089.

- [24] Y. Sumitomo, S. Tye, and S. S. Wong, *Statistical Distribution of the Vacuum Energy Density in Racetrack Kähler Uplift Models in String Theory*, *JHEP* **07** (2013) 052, [[arXiv:1305.0753](#)].
- [25] Y.-C. Qiu and S. H. H. Tye, *Linking the Supersymmetric Standard Model to the Cosmological Constant*, *JHEP* **01** (2021) 117, [[arXiv:2006.16620](#)].
- [26] L. Hui, J. P. Ostriker, S. Tremaine, and E. Witten, *Ultralight scalars as cosmological dark matter*, *Phys. Rev. D* **95** (2017), no. 4 043541, [[arXiv:1610.08297](#)].
- [27] S. H. H. Tye and S. S. C. Wong, *Linking Light Scalar Modes with A Small Positive Cosmological Constant in String Theory*, *JHEP* **06** (2017) 094, [[arXiv:1611.05786](#)].
- [28] C. Pitrou, A. Coc, J.-P. Uzan, and E. Vangioni, *Precision big bang nucleosynthesis with improved Helium-4 predictions*, *Phys. Rept.* **754** (2018) 1–66, [[arXiv:1801.08023](#)].
- [29] L. Pogosian, G.-B. Zhao, and K. Jedamzik, *Recombination-independent determination of the sound horizon and the Hubble constant from BAO*, *Astrophys. J. Lett.* **904** (2020), no. 2 L17, [[arXiv:2009.08455](#)].
- [30] S. M. Carroll, G. B. Field, and R. Jackiw, *Limits on a Lorentz and Parity Violating Modification of Electrodynamics*, *Phys. Rev. D* **41** (1990) 1231.
- [31] S. M. Carroll and G. B. Field, *The Einstein equivalence principle and the polarization of radio galaxies*, *Phys. Rev. D* **43** (1991) 3789.
- [32] D. Harari and P. Sikivie, *Effects of a Nambu-Goldstone boson on the polarization of radio galaxies and the cosmic microwave background*, *Phys. Lett. B* **289** (1992) 67–72.
- [33] S. A. Levshakov, M. G. Kozlov, and I. I. Agafonova, *Constraints on the electron-to-proton mass ratio variation at the epoch of reionization*, *Mon. Not. Roy. Astron. Soc.* **498** (2020), no. 3 3624–3632, [[arXiv:2008.11143](#)].
- [34] W. Hu, R. Barkana, and A. Gruzinov, *Cold and fuzzy dark matter*, *Phys. Rev. Lett.* **85** (2000) 1158–1161, [[astro-ph/0003365](#)].
- [35] H.-Y. Schive, T. Chiueh, and T. Broadhurst, *Cosmic Structure as the Quantum Interference of a Coherent Dark Wave*, *Nature Phys.* **10** (2014) 496–499, [[arXiv:1406.6586](#)].
- [36] D. J. E. Marsh, *Axion Cosmology*, *Phys. Rept.* **643** (2016) 1–79, [[arXiv:1510.07633](#)].
- [37] E. Aver, K. A. Olive, and E. D. Skillman, *The effects of He I $\lambda 10830$ on helium abundance determinations*, *JCAP* **07** (2015) 011, [[arXiv:1503.08146](#)].
- [38] R. J. Cooke, M. Pettini, and C. C. Steidel, *One Percent Determination of the Primordial Deuterium Abundance*, *Astrophys. J.* **855** (2018), no. 2 102, [[arXiv:1710.11129](#)].
- [39] L. Sbordone et al., *The metal-poor end of the Spite plateau. 1: Stellar parameters, metallicities and lithium abundances*, *Astron. Astrophys.* **522** (2010) A26, [[arXiv:1003.4510](#)].

- [40] B. D. Fields, *The primordial lithium problem*, *Ann. Rev. Nucl. Part. Sci.* **61** (2011) 47–68, [arXiv:1203.3551].
- [41] S. Hayakawa et al., *Experimental Study on the ${}^7\text{Be}(n, p){}^7\text{Li}$ and the ${}^7\text{Be}(n, \alpha){}^4\text{He}$ Reactions for Cosmological Lithium Problem*, *JPS Conf. Proc.* **31** (2020) 011036.
- [42] S. Ishikawa et al., *Experimental Study of the ${}^7\text{Be}(n, p_1){}^7\text{Li}^*$ Reaction for the Cosmological Lithium Problem*, *JPS Conf. Proc.* **31** (2020) 011037.
- [43] M. Clara and C. Martins, *Primordial nucleosynthesis with varying fundamental constants: Improved constraints and a possible solution to the Lithium problem*, *Astron. Astrophys.* **633** (2020) L11, [arXiv:2001.01787].
- [44] C. Iliadis and A. Coc, *Thermonuclear reaction rates and primordial nucleosynthesis*, *Astrophys. J.* **901** (2020), no. 2 127, [arXiv:2008.12200].
- [45] R. P. Gupta, *Do varying physical constants provide solution to the lithium problem?*, arXiv:2010.13628.
- [46] **Particle Data Group** Collaboration, P. Zyla et al., *Review of Particle Physics*, *PTEP* **2020** (2020), no. 8 083C01.
- [47] B. D. Fields, K. A. Olive, T.-H. Yeh, and C. Young, *Big-Bang Nucleosynthesis After Planck*, *JCAP* **03** (2020) 010, [arXiv:1912.01132].
- [48] A. Walker-Loud, *Nuclear Physics Review*, *PoS LATTICE2013* (2014) 013, [arXiv:1401.8259].
- [49] V. Flambaum and R. B. Wiringa, *Dependence of nuclear binding on hadronic mass variation*, *Phys. Rev. C* **76** (2007) 054002, [arXiv:0709.0077].
- [50] J. Berengut, V. Flambaum, and V. Dmitriev, *Effect of quark-mass variation on big bang nucleosynthesis*, *Phys. Lett. B* **683** (2010) 114–118, [arXiv:0907.2288].
- [51] J. Lesgourgues and S. Pastor, *Neutrino mass from Cosmology*, *Adv. High Energy Phys.* **2012** (2012) 608515, [arXiv:1212.6154].
- [52] **eBOSS** Collaboration, S. Alam et al., *The Completed SDSS-IV extended Baryon Oscillation Spectroscopic Survey: Cosmological Implications from two Decades of Spectroscopic Surveys at the Apache Point observatory*, arXiv:2007.08991.
- [53] G.-B. Zhao et al., *The Completed SDSS-IV extended Baryon Oscillation Spectroscopic Survey: a multi-tracer analysis in Fourier space for measuring the cosmic structure growth and expansion rate*, arXiv:2007.09011.
- [54] Y. Wang et al., *The clustering of the SDSS-IV extended Baryon Oscillation Spectroscopic Survey DR16 luminous red galaxy and emission line galaxy samples: cosmic distance and structure growth measurements using multiple tracers in configuration space*, *Mon. Not. Roy. Astron. Soc.* **498** (2020), no. 3 3470–3483, [arXiv:2007.09010].

- [55] J. Hou et al., *The Completed SDSS-IV extended Baryon Oscillation Spectroscopic Survey: BAO and RSD measurements from anisotropic clustering analysis of the Quasar Sample in configuration space between redshift 0.8 and 2.2*, *Mon. Not. Roy. Astron. Soc.* **500** (2020), no. 1 1201–1221, [arXiv:2007.08998].
- [56] H. du Mas des Bourboux et al., *The Completed SDSS-IV Extended Baryon Oscillation Spectroscopic Survey: Baryon Acoustic Oscillations with Ly α Forests*, *Astrophys. J.* **901** (2020), no. 2 153, [arXiv:2007.08995].
- [57] F. Beutler, C. Blake, M. Colless, D. H. Jones, L. Staveley-Smith, L. Campbell, Q. Parker, W. Saunders, and F. Watson, *The 6df galaxy survey: baryon acoustic oscillations and the local hubble constant*, *Monthly Notices of the Royal Astronomical Society* **416** (Jul, 2011) 3017–3032.
- [58] A. J. Ross, L. Samushia, C. Howlett, W. J. Percival, A. Burden, and M. Manera, *The clustering of the SDSS DR7 main Galaxy sample – I. A 4 per cent distance measure at $z = 0.15$* , *Mon. Not. Roy. Astron. Soc.* **449** (2015), no. 1 835–847, [arXiv:1409.3242].
- [59] A. G. Riess, S. Casertano, W. Yuan, L. M. Macri, and D. Scolnic, *Large Magellanic Cloud Cepheid Standards Provide a 1% Foundation for the Determination of the Hubble Constant and Stronger Evidence for Physics beyond Λ CDM*, *Astrophys. J.* **876** (2019), no. 1 85, [arXiv:1903.07603].
- [60] K. C. Wong et al., *HOLiCOW – XIII. A 2.4 per cent measurement of H_0 from lensed quasars: 5.3 σ tension between early- and late-Universe probes*, *Mon. Not. Roy. Astron. Soc.* **498** (2020), no. 1 1420–1439, [arXiv:1907.04869].
- [61] M. Reid, J. Braatz, J. Condon, L. Greenhill, C. Henkel, and K. Lo, *The Megamaser Cosmology Project: I. VLBI observations of UGC 3789*, *Astrophys. J.* **695** (2009) 287–291, [arXiv:0811.4345].
- [62] W. L. Freedman et al., *The Carnegie-Chicago Hubble Program. VIII. An Independent Determination of the Hubble Constant Based on the Tip of the Red Giant Branch*, arXiv:1907.05922.
- [63] C. Potter, J. B. Jensen, J. Blakeslee, et al., *2018, American Astronomical Society Meeting Abstracts # 232* 232.
- [64] C. D. Huang et al., *A Near-infrared Period–Luminosity Relation for Miras in NGC 4258, an Anchor for a New Distance Ladder*, *Astrophys. J.* **857** (2018), no. 1 67, [arXiv:1801.02711].
- [65] H. Gil-Marín et al., *The clustering of galaxies in the SDSS-III Baryon Oscillation Spectroscopic Survey: BAO measurement from the LOS-dependent power spectrum of DR12 BOSS galaxies*, *Mon. Not. Roy. Astron. Soc.* **460** (2016), no. 4 4210–4219, [arXiv:1509.06373].

- [66] W. Hu, N. Sugiyama, and J. Silk, *The Physics of microwave background anisotropies*, *Nature* **386** (1997) 37–43, [[astro-ph/9604166](#)].
- [67] W. Hu and S. Dodelson, *Cosmic Microwave Background Anisotropies*, *Ann. Rev. Astron. Astrophys.* **40** (2002) 171–216, [[astro-ph/0110414](#)].
- [68] S. Kachru, R. Kallosh, A. D. Linde, and S. P. Trivedi, *De Sitter vacua in string theory*, *Phys. Rev. D* **68** (2003) 046005, [[hep-th/0301240](#)].
- [69] N. Cribiori, C. Roupec, T. Wrase, and Y. Yamada, *Supersymmetric anti-D3-brane action in the Kachru-Kallosh-Linde-Trivedi setup*, *Phys. Rev. D* **100** (2019), no. 6 066001, [[arXiv:1906.07727](#)].
- [70] S. Parameswaran and F. Tonioni, *Non-supersymmetric String Models from Anti-D3-/D7-branes in Strongly Warped Throats*, [arXiv:2007.11333](#).
- [71] B. Vercnocke and T. Wrase, *Constrained superfields from an anti-D3-brane in KKLT*, *JHEP* **08** (2016) 132, [[arXiv:1605.03961](#)].
- [72] I. Antoniadis, E. Dudas, D. Ghilencea, and P. Tziveloglou, *Non-linear MSSM*, *Nucl. Phys. B* **841** (2010) 157–177, [[arXiv:1006.1662](#)].
- [73] R. Kallosh, F. Quevedo, and A. M. Uranga, *String Theory Realizations of the Nilpotent Goldstino*, *JHEP* **12** (2015) 039, [[arXiv:1507.07556](#)].
- [74] M. P. Garcia del Moral, S. Parameswaran, N. Quiroz, and I. Zavala, *Anti-D3 branes and moduli in non-linear supergravity*, *JHEP* **10** (2017) 185, [[arXiv:1707.07059](#)].
- [75] Z. Komargodski and N. Seiberg, *From Linear SUSY to Constrained Superfields*, *JHEP* **09** (2009) 066, [[arXiv:0907.2441](#)].
- [76] E. Dudas and S. Lüst, *An update on moduli stabilization with antibrane uplift*, [arXiv:1912.09948](#).
- [77] J.-P. Uzan, *Varying Constants, Gravitation and Cosmology*, *Living Rev. Rel.* **14** (2011) 2, [[arXiv:1009.5514](#)].
- [78] M. S. Safronova, D. Budker, D. DeMille, D. F. J. Kimball, A. Derevianko, and C. W. Clark, *Search for New Physics with Atoms and Molecules*, *Rev. Mod. Phys.* **90** (2018), no. 2 025008, [[arXiv:1710.01833](#)].
- [79] T. Fujita, K. Murai, H. Nakatsuka, and S. Tsujikawa, *Detection of isotropic cosmic birefringence and its implications for axion-like particles including dark energy*, [arXiv:2011.11894](#).
- [80] S. Andriolo, S. Y. Li, and S. H. H. Tye, *The Cosmological Constant and the Electroweak Scale*, *JHEP* **10** (2019) 212, [[arXiv:1812.04873](#)].
- [81] C. Heymans et al., *Kids-1000 cosmology: Multi-probe weak gravitational lensing and spectroscopic galaxy clustering constraints*, 2020.

- [82] E. Di Valentino and S. Bridle, *Exploring the Tension between Current Cosmic Microwave Background and Cosmic Shear Data*, *Symmetry* **10** (2018), no. 11 585.
- [83] SDSS Collaboration, E. S. Rykoff et al., *redMaPPer I: Algorithm and SDSS DR8 Catalog*, *Astrophys. J.* **785** (2014) 104, [arXiv:1303.3562].
- [84] R. Hlozek, D. Grin, D. J. E. Marsh, and P. G. Ferreira, *A search for ultralight axions using precision cosmological data*, *Phys. Rev. D* **91** (2015), no. 10 103512, [arXiv:1410.2896].
- [85] R. Hlozek, D. J. E. Marsh, and D. Grin, *Using the Full Power of the Cosmic Microwave Background to Probe Axion Dark Matter*, *Mon. Not. Roy. Astron. Soc.* **476** (2018), no. 3 3063–3085, [arXiv:1708.05681].
- [86] T. Kobayashi, R. Murgia, A. De Simone, V. Iršič, and M. Viel, *Lyman- α constraints on ultralight scalar dark matter: Implications for the early and late universe*, *Phys. Rev. D* **96** (2017), no. 12 123514, [arXiv:1708.00015].
- [87] M. I. Khlopov, B. A. Malomed, and I. B. Zeldovich, *Gravitational instability of scalar fields and formation of primordial black holes*, *mnras* **215** (Aug., 1985) 575–589.
- [88] D. J. E. Marsh and P. G. Ferreira, *Ultra-Light Scalar Fields and the Growth of Structure in the Universe*, *Phys. Rev. D* **82** (2010) 103528, [arXiv:1009.3501].
- [89] N. F. Lepora, *Cosmological birefringence and the microwave background*, gr-qc/9812077.
- [90] A. Lue, L.-M. Wang, and M. Kamionkowski, *Cosmological signature of new parity violating interactions*, *Phys. Rev. Lett.* **83** (1999) 1506–1509, [astro-ph/9812088].
- [91] R. Antonucci, *Unified models for active galactic nuclei and quasars*, *Ann. Rev. Astron. Astrophys.* **31** (1993) 473–521.
- [92] T. Liu, G. Smoot, and Y. Zhao, *Detecting axionlike dark matter with linearly polarized pulsar light*, *Phys. Rev. D* **101** (2020), no. 6 063012, [arXiv:1901.10981].
- [93] A. Caputo, L. Sberna, M. Frias, D. Blas, P. Pani, L. Shao, and W. Yan, *Constraints on millicharged dark matter and axionlike particles from timing of radio waves*, *Phys. Rev. D* **100** (2019), no. 6 063515, [arXiv:1902.02695].
- [94] T. Fujita, R. Tazaki, and K. Toma, *Hunting Axion Dark Matter with Protoplanetary Disk Polarimetry*, *Phys. Rev. Lett.* **122** (2019), no. 19 191101, [arXiv:1811.03525].
- [95] Y. Chen, J. Shu, X. Xue, Q. Yuan, and Y. Zhao, *Probing Axions with Event Horizon Telescope Polarimetric Measurements*, *Phys. Rev. Lett.* **124** (2020), no. 6 061102, [arXiv:1905.02213].
- [96] B. Feng, H. Li, M. Li, and X. Zhang, *Gravitational leptogenesis and its signatures in CMB*, *Phys. Lett.* **B620** (2005) 27–32, [hep-ph/0406269].

- [97] G.-C. Liu, S. Lee, and K.-W. Ng, *Effect on cosmic microwave background polarization of coupling of quintessence to pseudoscalar formed from the electromagnetic field and its dual*, *Phys. Rev. Lett.* **97** (2006) 161303, [astro-ph/0606248].
- [98] J. Guena, M. Abgrall, D. Rovera, P. Rosenbusch, M. E. Tobar, P. Laurent, A. Clairon, and S. Bize, *Improved Tests of Local Position Invariance Using Rb-87 and Cs-133 Fountains*, *Phys. Rev. Lett.* **109** (2012) 080801, [arXiv:1205.4235].
- [99] C. M. Casey, D. Narayanan, and A. Cooray, *Dusty Star-Forming Galaxies at High Redshift*, *Phys. Rept.* **541** (2014) 45–161, [arXiv:1402.1456].
- [100] I. Ushijima, M. Takamoto, M. Das, T. Ohkubo, and H. Katori, *Cryogenic optical lattice clocks*, *Nature Photonics* **9** (2015), no. 3 185–189.
- [101] M. G. Kozlov, M. S. Safronova, J. R. Crespo López-Urrutia, and P. O. Schmidt, *Highly charged ions: Optical clocks and applications in fundamental physics*, *Rev. Mod. Phys.* **90** (2018), no. 4 045005, [arXiv:1803.06532].
- [102] C. J. Campbell, A. G. Radnaev, A. Kuzmich, V. A. Dzuba, V. V. Flambaum, and A. Derevianko, *A Single-Ion Nuclear Clock for Metrology at the 19th Decimal Place*, *Phys. Rev. Lett.* **108** (2012) 120802, [arXiv:1110.2490].
- [103] E. Peik, T. Schumm, M. S. Safronova, A. Pálffy, J. Weitenberg, and P. G. Thirolf, *Nuclear clocks for testing fundamental physics*, arXiv:2012.09304.
- [104] **TMT International Science Development Teams & TMT Science Advisory Committee** Collaboration, W. Skidmore et al., *Thirty Meter Telescope Detailed Science Case: 2015*, *Res. Astron. Astrophys.* **15** (2015), no. 12 1945–2140, [arXiv:1505.01195].
- [105] P. Behroozi et al., *The Universe at $z > 10$: predictions for JWST from the universemachine DR1*, *Mon. Not. Roy. Astron. Soc.* **499** (2020), no. 4 5702–5718, [arXiv:2007.04988].
- [106] D. W. Marsden et al., *The Atacama Cosmology Telescope: Dusty Star-Forming Galaxies and Active Galactic Nuclei in the Southern Survey*, *Mon. Not. Roy. Astron. Soc.* **439** (2014), no. 2 1556–1574, [arXiv:1306.2288].
- [107] X. Chen, S. P. Ellingsen, and Y. Mei, *Astrophysical constraints on the proton-to-electron mass ratio with FAST*, *Res. Astron. Astrophys.* **19** (2019) 18, [arXiv:1904.03871].
- [108] C. L. Carilli and S. Rawlings, *Science with the Square Kilometer Array: Motivation, key science projects, standards and assumptions*, *New Astron. Rev.* **48** (2004) 979, [astro-ph/0409274].
- [109] W. Ubachs, J. Bagdonaitė, E. J. Salumbides, M. T. Murphy, and L. Kaper, *Search for a drifting proton–electron mass ratio from H_2* , *Rev. Mod. Phys.* **88** (2016) 021003, [arXiv:1511.04476].

- [110] W. Hu and N. Sugiyama, *Small scale cosmological perturbations: An Analytic approach*, *Astrophys. J.* **471** (1996) 542–570, [[astro-ph/9510117](#)].
- [111] J. Chluba and R. Thomas, *Towards a complete treatment of the cosmological recombination problem*, *Mon. Not. Roy. Astron. Soc.* **412** (2011) 748, [[arXiv:1010.3631](#)].
- [112] J. A. Rubiño-Martín, J. Chluba, W. A. Fendt, and B. D. Wandelt, *Estimating the impact of recombination uncertainties on the cosmological parameter constraints from cosmic microwave background experiments*, *Monthly Notices of the Royal Astronomical Society* **403** (Mar, 2010) 439–452.
- [113] J. Chluba, *Could the cosmological recombination spectrum help us understand annihilating dark matter?*, *Monthly Notices of the Royal Astronomical Society* **402** (Feb, 2010) 1195–1207.
- [114] J. Chluba, G. M. Vasil, and L. J. Dursi, *Recombinations to the rydberg states of hydrogen and their effect during the cosmological recombination epoch*, *Monthly Notices of the Royal Astronomical Society* **407** (Jul, 2010) 599–612.
- [115] S. Seager, D. D. Sasselov, and D. Scott, *A new calculation of the recombination epoch*, *Astrophys. J. Lett.* **523** (1999) L1–L5, [[astro-ph/9909275](#)].
- [116] E. R. Switzer and C. M. Hirata, *Primordial helium recombination. 1. Feedback, line transfer, and continuum opacity*, *Phys. Rev. D* **77** (2008) 083006, [[astro-ph/0702143](#)].
- [117] D. Grin and C. M. Hirata, *Cosmological hydrogen recombination: The effect of extremely high-nstates*, *Physical Review D* **81** (Apr, 2010).
- [118] Y. Ali-Haïmoud and C. M. Hirata, *Ultrafast effective multilevel atom method for primordial hydrogen recombination*, *Physical Review D* **82** (Sep, 2010).